

RESEARCH ACTIVITIES V

Department of Applied Molecular Science

V-A Molecular Mechanisms of Oxygen Activation by Heme Enzymes

By sharing a common prosthetic group, the heme enzymes such as cytochrome P450s, peroxidases, and catalases catalyze their own unique biological functions; monooxygenation, hydrogen peroxide dependent oxidation, and dismutation of hydrogen peroxide, respectively. Our efforts have been focused on the elucidation of the structure-biological function relationship of those heme enzymes by employing both enzymic systems including mutants and their model systems.

V-A-1 Formation and Catalytic Roles of Compound I in the Hydrogen Peroxide-Dependent Oxidation by His64 Myoglobin Mutants

MATSUI, Toshitaka; OZAKI, Shin-ichi; WATANABE, Yoshihito

[*J. Am. Chem. Soc.* in press]

A His64 → Asp mutant of sperm whale myoglobin (Mb), H64D Mb, has been prepared to mimic the active site of chloroperoxidase from the marine fungus *Caldariomyces fumago*, in which distal glutamic acid is suggested to enhance the compound I formation by H₂O₂. The H64D mutant allows us to see the accumulation of compound I in the reaction of Mb with H₂O₂ for the first time (Figure 1). The successful observation of compound I is due to at least 50-fold improvement in the formation rate of compound I as well as its stabilization upon the His64 → Asp replacement. Catalytic activity of wild type Mb and a series of His64 Mb mutants (H64A, H64S, H64L, and H64D Mb) are examined for one-electron oxidation and oxygenation by using H₂O₂ as an oxidant. The H64D mutant is the best catalyst among the myoglobins and shows 50 ~ 70-fold and 600 ~ 800-fold higher activity than the wild type in the one-electron oxidations and peroxygenations, respectively. The origin of the varied activity upon the mutations are discussed on the basis of the formation rate and stability of compound I.

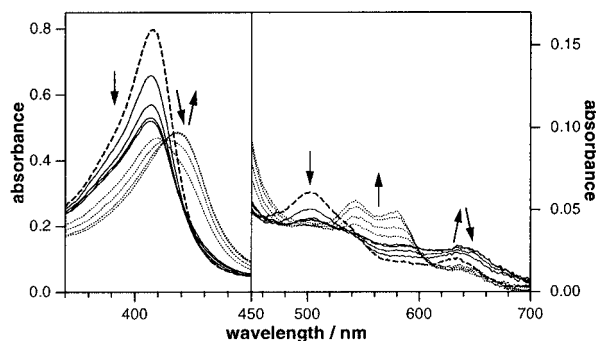


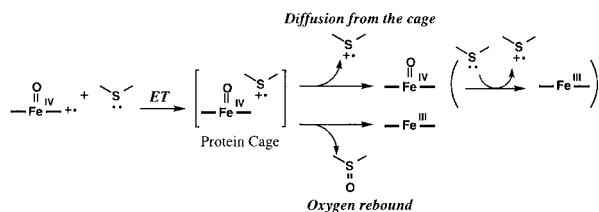
Figure 1. Spectral changes of H64D Mb in the reactions with 1 mM H₂O₂ at pH 7.0 and 20 °C. The spectra were recorded before mixing (broken line), at 10, 30, 60, 100, and 150 ms (solid lines), and at 1, 2, 4, and 6 sec (dotted lines) after mixing. For clarity, Soret and Visible regions are expanded and magnified, respectively.

V-A-2 The Mechanisms of *N*-Demethylation Catalyzed by Heme Enzymes: Mechanisms of Sulfoxidation Catalyzed by High-Valent Intermediates of Heme Enzymes: Electron Transfer vs Oxygen Transfer Mechanism

GOTO, Yoshio; MATSUI, Toshitaka; OZAKI, Shin-ichi; WATANABE, Yoshihito; FUKUZUMI, Shunichi¹ (¹Osaka Univ.)

[*J. Am. Chem. Soc.* in press]

Mechanisms of sulfoxidation catalyzed by high-valent intermediates of heme enzymes have been investigated by direct observation of sulfide induced reduction of three different compound I species including HRP (horseradish peroxidase), the His64Ser myoglobin (Mb) mutant and O=Fe^{IV}TMP²⁺ (**1**) (TMP = 5,10,15,20-tetramesitylporphyrin dianion). The reaction of thioanisole and compound I of HRP (10 mM, pH 7.0, 298 K) gives the resting state of HRP with accumulation of compound II as an intermediate. The yield of sulfoxide by a stoichiometric reaction of HRP compound I with thioanisole was only 25 ± 5%. On the other hand, the same sulfoxidation by both **1** and His64Ser Mb compound I exclusively exhibited a two-electron process resulting in quantitative formation of sulfoxide. When 1,5-dithiacyclooctane (DTCO) is employed as a substrate, the reaction of His64Ser Mb compound I with DTCO exhibits rapid formation of compound II which decays to the ferric state due to the low oxidation potential of DTCO. The observed rate constants (log *k*_{obs}) of the reactions of **1** and compounds I of HRP and His64Ser Mb with a series of *p*-substituted thioanisoles correlate with the one-electron oxidation potentials (*E*⁰_{ox}) of the sulfides. A comparison of these correlations with the established correlation between log *k*_{obs} and *E*⁰_{ox} for the corresponding electron transfer reactions of substituted *N,N*-dimethylanilines has revealed that the sulfoxidation reactions of compound I of HRP with the sulfides proceed via electron transfer while the sulfoxidations catalyzed by **1** and compound I of His64Ser Mb occur via direct oxygen transfer.



Scheme 1. Electron Transfer vs. Direct Oxygen Transfer.

V-A-3 Effects of the Arrangement of a Distal Catalytic Residue on Regioselectivity and Reactivity in the Coupled Oxidation of Sperm Whale Myoglobin Mutants

MURAKAMI, Tatsuya¹; MORISHIMA, Isao¹; MATSUI, Toshitaka; OZAKI, Shin-ichi; HARA, Isao; YANG, Hui-Jun; WATANABE, Yoshihito
(¹Kyoto Univ.),

[*J. Am. Chem. Soc.* **121**, 2007 (1999)]

Heme oxygenase is a central monooxygenase of the heme catabolism and forms a stoichiometric complex

with protoheme IX. The enzyme utilizes electrons and molecular oxygen for the regioselective heme degradation to afford α -biliverdin and carbon monoxide (CO) through three sequential oxygenase reactions. To understand factors which control the high regioselectivity, the regiospecific heme degradation of sperm whale myoglobin (Mb) mutants has been performed L29H/H64L myoglobin (Mb) almost exclusively gives biliverdin IX γ although H64L and wild type Mb mainly affords the α -isomer. Relocation of the distal histidine at the 43, and 107 position increases the amount of γ -isomer to 44 and 22%, respectively. Interestingly, the increase in the ratio of γ -isomer is also observed by a single replacement of either His-64 with Asp or Phe-43 with Trp. It appears that the polarity of the active site as well as hydrogen bonding between oxygen molecule bound to the heme iron and His or Trp is important in controlling the regioselectivity. The results of coupled oxidation kinetics, autooxidation kinetics, and redox potential of Fe³⁺/Fe²⁺ couple are discussed with regards to their implications for the active site and mechanism of heme oxygenase.

V-B Model Studies of Non-Heme Proteins

Non-heme proteins play important roles in biological redox processes. Many reactions catalyzed by the non-heme enzymes are quite similar to those by hemoproteins. We are interested in the active intermediates responsible for oxidation and oxygenation by non-heme enzyme, especially the similarity and differences.

V-B-1 A Model for Peroxo Intermediates in Reactions Catalyzed by Non-Heme Iron Enzymes

WADA, Akira¹; OGO, Seiji; WATANABE, Yoshihito; MUKAI, Masahiro; KITAGAWA, Teizo; JITSUKAWA, Koichiro¹; MASUDA, Hideki¹; EINAGA, Hisahiko¹
(¹Nagoya Inst. Tech.)

[*Inorg. Chem.* **38**, 3592 (1999)]

Thermodynamically extremely stable alkylperoxo-iron(III) complexes have first been prepared from reaction of the ternary iron(III) complex with a tripodal pyridylamine ligand, bis(6-pivalamido-2-pyridylmethyl)(2-pyridylmethyl)amine (BPPA), and trimethylacetate with alkylperoxide (*t*BuOO or C₆H₅C(CH₃)OO) in MeCN. The structure of the starting complex [Fe(bppa)(*t*BuCOO)](ClO₄)₂ (**1**) was determined by X-ray diffraction method. The electronic absorption spectra obtained by addition of aqueous solutions containing *t*BuOOH (TBHP) (69 w/w%) or C₆H₅C(CH₃)OOH (CHP) (80 w/w%) to **1** showed characteristic bands at 613 nm ($\epsilon = 2000 \text{ M}^{-1}\text{cm}^{-1}$) or 585 nm ($\epsilon = 2200 \text{ M}^{-1}\text{cm}^{-1}$) assignable to an alkylperoxide-iron(III) charge transfer transition, respectively. The resonance Raman spectra revealed strong resonance-enhanced Raman features at 873, 838, 629, and 469 cm⁻¹ and 878, 838, 639, 548, and 493 cm⁻¹, respectively. The ESI-mass spectra afforded positive and negative ion peaks at $m/z = 316.5$ and 932 corresponding to the ions, [Fe(bppa)(*t*BuOO)]²⁺ and {[Fe(bppa)(*t*BuOO)](ClO₄)₃}⁻, and at $m/z = 347.5$

and 994 assignable to [Fe(bppa)(C₆H₅C(CH₃)OO)]²⁺ and {[Fe(bppa)(C₆H₅C(CH₃)OO)](ClO₄)₃}⁻, respectively. The ESR spectra at 77 K demonstrated a typical high spin iron(III) state with small rhombic distortion ($g = 7.58, 5.81, 4.25, 1.82, E/D = 0.067$ and $g = 7.76, 5.65, 4.20, 1.78, E/D = 0.070$, respectively). The cyclic voltammetry of the starting complex **1** exhibited a quasi-reversible redox wave of the Fe^{3+/2+} couple at +700 mV vs NHE that is fairly agreement with that in lipoxygenase. Their alkylperoxide complexes were successfully isolated as powder precipitates, and the UV-Vis, ESR, and ESI-mass spectra of the acetone or MeCN solutions containing the precipitates were almost the same as those in solution. The above findings strongly suggest that the reaction of **1** with alkylperoxide generated the extremely stable iron(III)-alkylperoxide complexes with seven-coordinate.

V-B-2 An Unusual Conversion of a Ni(III)₂(μ -O)₂ Core into a Ni(II)₂(μ -OO)₂ Core by H₂O₂ and Oxygenation of Ligand

SHIREN, Kazushi¹; OGO, Seiji; FUJINAMI, Shuhei¹; HAYASHI, Hideki¹; SUZUKI, Masatatsu¹; UEHARA, Akira¹; WATANABE, Yoshihito; MORO-OKA, Yoshihiko²
(¹Kanazawa Univ.; ²Tokyo Inst. Tech.)

[*J. Am. Chem. Soc.* in press]

A six-coordinate bis(μ -oxo)nickel(III) complex, [Ni₂(μ -O)₂(Me₃-tpa)₂]²⁺ (**1**), was synthesized by

reaction of $[\text{Ni}_2(\mu\text{-OH})_2(\text{Me}_3\text{-tpa})_2]^{2+}$ (**2**) with 1 equiv. of hydrogen peroxide in methanol at -90°C , where $\text{Me}_3\text{-tpa}$ = tris(6-methyl-2-pyridylmethyl)amine. The 6-methyl groups of $\text{Me}_3\text{-tpa}$ have a significant influence on the formation and stabilization of the high-valent bis(μ -oxo)dinickel(III) species. Reaction of **2** with a large excess of hydrogen peroxide (> 10 equiv.) afforded a novel bis(μ -superoxo)dinickel(II) complex, $[\text{Ni}_2(\mu\text{-O}_2)_2(\text{Me}_3\text{-tpa})_2]^{2+}$ (**3**). The reaction demonstrates a unique conversion of a $\text{Ni}^{\text{III}}(\mu\text{-O})_2\text{Ni}^{\text{III}}$ core into a $\text{Ni}^{\text{II}}(\mu\text{-OO})_2\text{Ni}^{\text{II}}$ core upon exposure to hydrogen peroxide. Complexes **1**, **2**, and **3** were characterized by X-ray crystallography and various physicochemical techniques. Complex **1** has an edge-shared bioctahedral structure with a $\text{Ni}(\mu\text{-O})_2\text{Ni}$ core. Each nickel atom is coordinated by $\text{Me}_3\text{-tpa}$ to complete a distorted octahedral coordination sphere. The average Ni–O and Ni–N bond distances of **1** (1.871 and 2.143 Å, respectively) are significantly shorter than those of **2**, (2.018 and 2.185 Å, respectively), suggesting that **1** is a bis(μ -oxo)dinickel(III) complex. The crystal structure of **3** consists of a centrosymmetric $\text{Ni}(\mu\text{-OO})_2\text{Ni}$ core with $\text{Me}_3\text{-tpa}$ nitrogens. The nickel centers are in a distorted octahedral structure and linked by two $\mu\text{-1,2-O-O}$ bridges to form a six-membered ring with a chair conformation. The O–O bond distance is 1.345(6) Å, which is intermediate between those of the typical peroxo and superoxo complexes. The resonance Raman spectrum of a powdered sample of **3** measured at 110 K showed an isotope-sensitive band at 1096 cm^{-1} (1044 cm^{-1} for an ^{18}O labeled sample), indicating that **3** is a bis(μ -superoxo) $\text{Ni}_2(\text{II})$ complex. Thermal decomposition of both **1** and **3** in acetone at -20°C under N_2 atmosphere resulted in a partial hydroxylation of a methyl group of $\text{Me}_3\text{-tpa}$ in yield of 21–29% for both complexes. A carboxylate complex, $[\text{Ni}(\text{Me}_2\text{-tpaCOO})\text{-}(\text{OH}_2)]^+$ (**4**), where one of the three methyl groups of $\text{Me}_3\text{-tpa}$ is oxidized to carboxylate, was isolated from the decomposition under N_2 atmosphere. During the decomposition process, dioxygen evolution was simultaneously observed in yield of $35 \pm 4\%$. Thermal decomposition of **1** under O_2 atmosphere also gave **4**. The Electrospray ionization mass spectrometry (ESIMS) of **3** revealed the formation of **1** during the decomposition process. These results suggest that one possible decomposition pathway of **3** is a disproportionation of two coordinated superoxides to dioxygen and peroxide followed by the O–O bond scission of peroxide to regenerate **1**, which is responsible to the hydroxylation and the oxidation of the 6-methyl group of $\text{Me}_3\text{-tpa}$.

V-B-3 Structural and Functional Model Complexes for the Catechol-Bound Intermediate of Intradiol-Cleaving Catechol Dioxygenases

YAMAHARA, Ryo¹; OGO, Seiji; WATANABE, Yoshihito; FUNABIKI, Takuzo²; JITSUKAWA,

Koichiro¹; MASUDA, Hideki¹; EINAGA, Hisahiko¹
(¹Nagoya Inst. Tech.; ²Kyoto Univ.)

[*Inorg. Chim. Acta* in press]

This paper reports the synthesis and structures of (catecholato)iron(III) complexes with tetradentate tripodal ligands ($\text{L}_{\text{R}',\text{R}''} = \{2\text{-hydroxy-3-R}'\text{-5-R}''\text{-phenyl-bis(2-pyridylmethyl)amine}\}$) containing substituted phenol and pyridine units: $[\text{Fe}^{\text{III}}(\text{L}_{\text{R}',\text{R}''})\text{(DBC)}]$ (**1a**: $\text{R}',\text{R}'' = \text{H,H}$, **1b**: $\text{R}',\text{R}'' = \text{Me,Me}$, and **1c**: $\text{R}',\text{R}'' = \text{H,Cl}$, DBC = 3,5-di-*tert*-butylcatechol). X-ray structure analysis has revealed that the coordination arrangement around the iron atom of **1a** is very similar to that proposed for the active site of the catechol-bound intermediate of protocatechuate 3,4-dioxygenase (3,4-PCD). The series of complex **1** derivatives has been synthesized by two different methods: (i) reaction of $[\text{Fe}^{\text{III}}(\text{L}_{\text{R}',\text{R}''})\text{(acac)}]^+$ (**2a**: $\text{R}',\text{R}'' = \text{H,H}$, **2b**: $\text{R}',\text{R}'' = \text{Me,Me}$, and **2c**: $\text{R}',\text{R}'' = \text{H,Cl}$, acac = acetylacetonate) with 1 equiv. of DBC and 1 equiv. of Et_3N in *N,N*-dimethylformamide, and (ii) reaction of $[\text{Fe}^{\text{III}}(\text{L}_{\text{R}',\text{R}''})\text{Cl}_2]$ (**3a**: $\text{R}',\text{R}'' = \text{H,H}$, **3b**: $\text{R}',\text{R}'' = \text{Me,Me}$, and **3c**: $\text{R}',\text{R}'' = \text{H,Cl}$) with 2 equiv. of AgOTf ($\text{OTf} = \text{O}_3\text{SCF}_3^-$), 1 equiv. of the catechols, and 2 equiv. of Et_3N in DMF. The exogenous acac ligand of **2** acts as a Lewis-base like the Tyr447 ligand in the active site of 3,4-PCD in the formation of the catechol-bound intermediate. Complexes **1**, **2**, and **3** have been characterized by X-ray analysis, visible and EPR spectroscopies, and cyclic voltammetry. Oxygenation of the bound DBC on **1** in the presence of O_2 has also been investigated and is discussed based on the Lewis basicity of the tripodal ligand containing the substituted phenolato group which is introduced to mimic the Tyr408 ligand of 3,4-PCD.

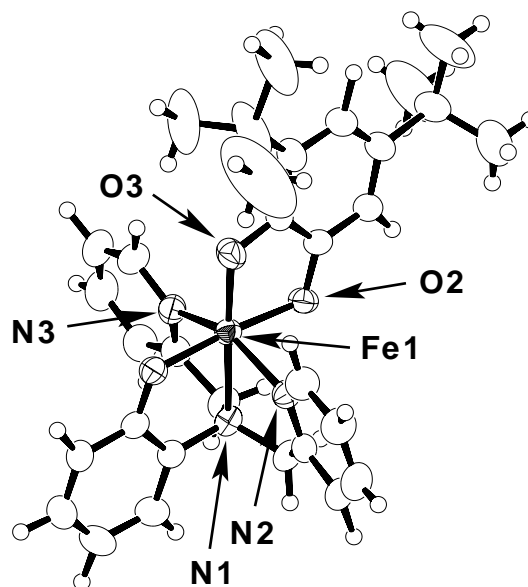


Figure 1. ORTEP drawing of **1a**.

V-C Transition Metal Oxide Clusters

Organometallic oxide clusters with cubic and incomplete cubic frameworks have useful applications as homogeneous and heterogeneous catalysts for reactions such as the oxidation and metathesis of propene. Understanding of the formation mechanisms of such oxide clusters may lead to the further development of synthetic methodologies for the construction of desired clusters having efficient catalytic ability for hydrocarbon transformations.

V-C-1 Direct Observation by Electrospray Ionization Mass Spectrometry of a Key Intermediate in the Formation of a Double Bookshelf-Type Oxide Cluster

TAKARA, Satoshi¹; OGO, Seiji; NISHIKAWA, Koji¹; KINOSHITA, Isamu¹; ISOBE, Kiyoshi¹; WATANABE, Yoshihito
(¹Osaka City Univ.)

[*Angew. Chem., Int. Ed. Engl.* in press]

We have found that a 1:4 reaction of [$[\text{Cp}^*\text{Rh}(\text{m-Cl})\text{Cl}]_2$] (**1**) and [$(n\text{Bu})_4\text{N}]_2[\text{Mo}_2\text{O}_7]$] (**2**) in MeOH

quantitatively yields a double bookshelf-type oxide cluster [$(n\text{Bu})_4\text{N}]_2[(\text{Cp}^*\text{Rh})_2\text{Mo}_6\text{O}_{20}(\text{OMe})_2]$ (**3**) with a multi-incomplete cubic framework. We have investigated the formation mechanism of **3** by electrospray ionization mass spectrometry (ESI-MS) which allows us to detect unstable species generated in solution. Herein, we report a direct observation by ESI-MS of [$\text{Cp}^*\text{RhMo}_3\text{O}_8(\text{OMe})_5$]⁻ (**3_{im}**; m/z 809), a key intermediate in the formation of **3** from the reaction of **1** and **2** in MeOH at -78 °C. Time dependent-behavior of selected ions during the reaction of **1** and **2** was monitored by rapid scanning of ESI-MS. The existence of the methoxo ligands in **3_{im}** was confirmed by isotopic labeling experiments.

V-D Aqueous Organometallic Chemistry

In recent years, aqueous organometallic chemistry has been widely studied because of industrial advantages and environmental concerns. Few organometallic aqua complexes have been, until now, isolated and used as water-soluble reagents in aqueous media. We have investigated a homogeneous hydrogenation in aqueous media using organometallic aqua complexes whose structures and properties drastically change as a function of pH because of deprotonation of the aqua ligands.

V-D-1 A Unique pH-Dependent Transfer Hydrogenation of Water-Soluble Carbonyl Compounds with an Organometallic Aqua Complex as a Catalyst Precursor in Water

OGO, Seiji; MAKIHARA, Nobuyuki; WATANABE, Yoshihito

[*Organometallics* in press]

This paper reports a unique pH-dependent hydrogen transfer from HCOONa to water-soluble carbonyl compounds with an organometallic aqua complex [$\text{Cp}^*\text{Ir}^{\text{III}}(\text{H}_2\text{O})_3$]²⁺ (**1**, Cp* = $\eta^5\text{-C}_5\text{Me}_5$) as a catalyst precursor in water. The structure of **1** was unequivocally determined by X-ray analysis. Complex **1** is deprotonated to form a dinuclear complex [$(\text{Cp}^*\text{Ir}^{\text{III}})_2(\mu\text{-OH})_3$]⁺ (**2**) at pH 3.2. ¹H NMR, IR, and electrospray ionization mass spectrometry (ESI-MS) experiments show that the active species in this catalytic reaction is a dinuclear μ -hydride complex [$(\text{Cp}^*\text{Ir}^{\text{III}})_2(\mu\text{-H})(\mu\text{-OH})(\mu\text{-HCOO})$]⁺ (**3**). The rate of this transfer hydrogenation shows a sharp maximum at pH 3.2. The series of carbonyl compounds used in this catalytic reaction are a straight chain aldehyde (*n*-butyraldehyde), a cyclic aldehyde (cyclopropanecarboxaldehyde), a ketone (2-butanone), an aldehyde-acid (glyoxylic acid), and a keto-acid (pyruvic acid).

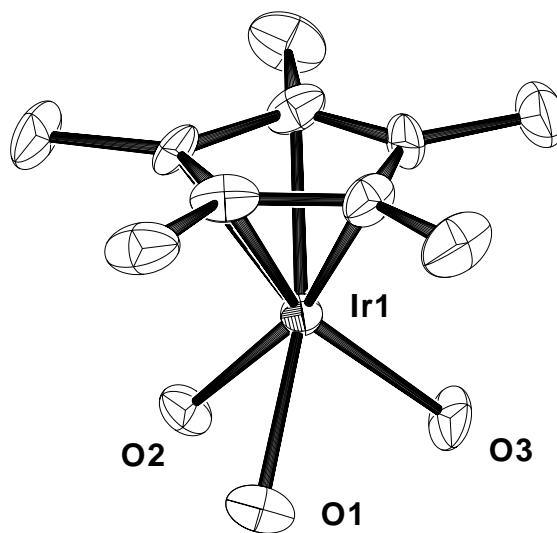


Figure 1. ORTEP drawing of **1**.

V-E Synthesis of New High-spin Molecule

Design and synthesis of organic molecules with high-spin ground states are current subjects of great importance. When three unpaired electrons are placed in proximity and allowed to interact magnetically, 1,3,5-Benzenetriyl unit can be deemed superior to *m*-phenylene unit in assembling organic free radical centers in higher concentrations within a molecule and aligning those spins in parallel for the purpose of designing and constructing very high-spin organic molecules. While some 1,3,5-trisubstituted benzene derivatives having nitronyl nitroxides, diarylmethyl radicals, diphenylamine cation radicals, phenylcarbene, and nitrenes as substituents are reported to be with high-spin ground states, they are either not persistent under ambient conditions or the intraradical couplings are not strong enough in magnitude.

V-E-1 Structure and Magnetic Property of the Organic Triradical with Triazine Skeleton; 1,3,5-Tris(*p*-(*N*-oxy-*N*-*tert*-butylamino)-phenyl)triazine

HAYAMI, Shinya; INOUE, Katsuya

[*Chem. Lett.* 545 (1999)]

1,3,5-tris(*p*-(*N*-oxy-*N*-*tert*-butylamino)phenyl)benzene has been known as persistent triradical with quartet ground state. New triradical with triazine skeleton was synthesized and characterized. Nitroxide triradical with triazine derivative 1,3,5-tris(*p*-(*N*-oxy-*N*-*tert*-butylamino)phenyl)triazine (**1**) exhibits stronger intramolecular ferromagnetic interaction than that with benzene derivative 1,3,5-tris(*p*-(*N*-oxy-*N*-*tert*-butylamino)phenyl)-benzene (**2**), the magnitude of the interactions depends on the planarity of the structures and/or on the spin density of center skeletons. Temperature dependence of the effective magnetic moments values observed for crystalline **1** in 1.8–350 K. The simulation of an isosceles-triangular exchange coupling model gave $J_1/k_B = 14.7$ K, $\gamma = 0.87$, and $\theta = -5.43$ K.

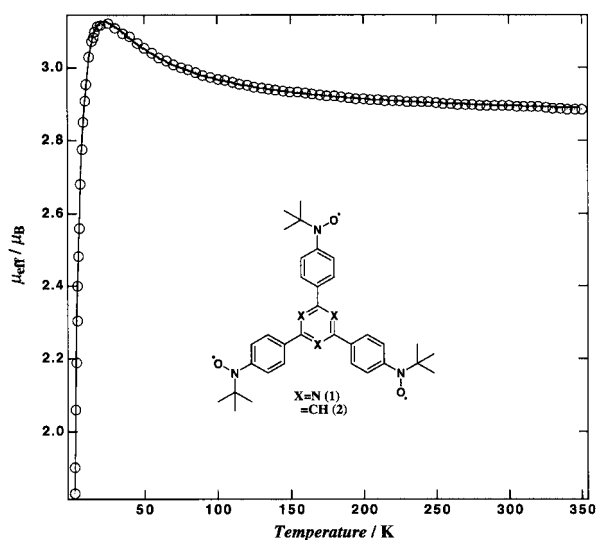


Figure 1. Temperature dependence of effective magnetic moment μ_{eff} values of **1** in neat crystals. Solid curve is a theoretical one.

V-F Construction of New Molecule-Based Magnets

Construction of molecular based magnetic materials which have well-defined one- or two-dimensional magnetic structure is a scientific subject of increasing interest. Heterospin systems consisting of paramagnetic transition metal ions and organic free radicals as ligands constitute one of the mainstreams of such studies. Several of these materials have been established to have finite critical temperature of a ferro- or ferrimagnetic transition.

We have introduced a new strategy of employing π -conjugated polyaminoxyls as ligands in which the $2p$ -spins of the NO groups interact ferromagnetically ($J_1 > 0$). The dimensionality of the complex and the sign and magnitude of the exchange coupling between the neighboring spins may be readily tuned by this strategy. Depending on the nature of the additional interchain or interlayer interaction, the polymers are expected to become an antiferromagnet or ferri/ferromagnet. By modifying and extending this design strategy to bis- and tris(aminoxyl) radicals having triplet and quartet ground states, respectively, we have been able to construct with the aid of magnetic metal ions one-dimensional (1D) chain, two-dimensional (2D) network and three-dimensional (3D) parallel-crosses structures in which both the organic $2p$ and metallic $3d$ spins have been ordered in macroscopic scales. Since such a rational approach by self-assembly to the tailored extended systems having relevant physical properties is of great importance in materials synthesis.

V-F-1 One-Dimensional Ferro- and Ferri-magnetic Chains Made up of an Alternating Array of 1,3-Bis(*N*-*tert*-Butyl-*N*-oxy-amino)-benzene Derivatives and Mn(II)(hfac)₂

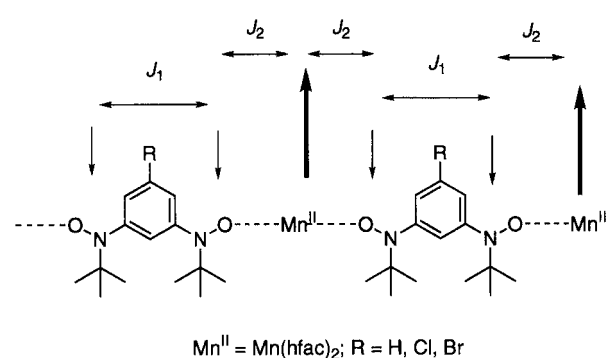
INOUE, Katsuya; IWAHORI, Fumiyasu¹; MARKOSYAN, Ashot S.^{2,3}; IWAMURA, Hiizu⁴
(¹GUAS.; ²M. V. Lomonosov Moscow State Univ.; ³IMS;

⁴Kyushu Univ.)

[*Coord. Chem. Rev.* in press]

Bis(hexafluoroacetylacetonato) manganese (II), Mn(hfac)₂, reacts with the bisnitroxide radicals, 5-R-1,3-Bis(*N*-*tert*-butyl-*N*-oxyamino)benzene **1_R** (R = H, Cl and Br), yielding 1-dimensional polymeric complexes

of formula $[\text{Mn}(\text{hfac})_2\mathbf{1}_R]_n$. X-ray analysis of the complexes has shown that they crystallize in the monoclinic, space group $P2_1/n$. In this structure, the manganese(II) ions and $\mathbf{1}_R$ molecules make up 1-D chains with the bisnitroxide radical serving as a bidentate ligand to $\text{Mn}(\text{II})(\text{hfac})_2$. The $\mathbf{1}_H$ complex orders antiferromagnetically at 5.5 K, while the $\mathbf{1}_{Cl}$ and $\mathbf{1}_{Br}$ complexes show ferrimagnetic order at 4.8 and 5.3 K, respectively. The intrachain exchange interaction parameters for a model of $S = 3/2$ ferromagnetic chains were found to be, $2J_{\text{eff}}/k = 23 \pm 2$ K in all the compounds. J_{eff} means effective magnetic exchange interaction between units of NO-Mn-NO . A change in the sign of the interchain exchange interaction is referred to the change of the shortest exchange path, from the $\text{Mn-F-N}(\text{tert-Bu})\text{O} \cdot (\mathbf{1}_{Cl}$ and $\mathbf{1}_{Br})$ to $\text{N}(\text{tert-Bu})\text{O} \cdot \text{F-N}(\text{tert-Bu})\text{O} \cdot (\mathbf{1}_H)$.



Scheme 1.

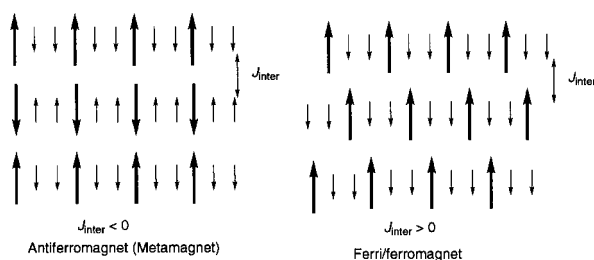


Figure 1. Schematic drawing of magnetic structure for the complex a) $\text{Mn}(\text{hfac})_2\mathbf{1}_H$, b) $\text{Mn}(\text{hfac})_2\mathbf{1}_{Cl}$ and $\text{Mn}(\text{hfac})_2\mathbf{1}_{Br}$.

V-F-2 Influence of the Thermal Excitations of the Ferrimagnetic $(\bar{1}/2, 5/2, \bar{1}/2)$ Linear Trimer on the Paramagnetic Behavior of the Layered Metal-Radical Complex $\{\text{Mn}(\text{hfac})_2\}_3(\text{R}_N)_2 \cdot n\text{-C}_7\text{H}_{16}$

HOSOKOSHI, Yuko; INOUE, Katsuya; MARKOSYAN, Ashot S.^{1,2}
(¹IMS; ²M. V. Lomonosov Moscow State Univ.)

[Phys. Lett. A in press]

The complex $\{\text{Mn}(\text{hfac})_2\}_3(\mathbf{3R}_\Delta)_2 \cdot n\text{-C}_7\text{H}_{16}$ forms a two-dimensional honeycomb-like spin network. It is shown that the spins of $\text{Mn}(\text{II})$ form with the two $1/2$ -spins of different adjacent triradicals $\mathbf{3R}_\Delta$ linear $(\bar{1}/2, 5/2, \bar{1}/2)$ ferrimagnetic trimers, which determine the paramagnetic properties of the complex. The intratrimer excitations result in the decay of the trimers above 140 K.

The experimental data can well be described within this model both at high and low temperatures thus proving the importance of the thermal excitations within the trimers. The best agreement was obtained at $J_{\text{TR}}/k_B = -176.4$ K and $= +0.333$ emu/mol. The power series expansion for the 2D honeycomb network gives $J_{\text{TR}}/k_B = -175.4$ K and $J_1/k_B = +0.226$ K.

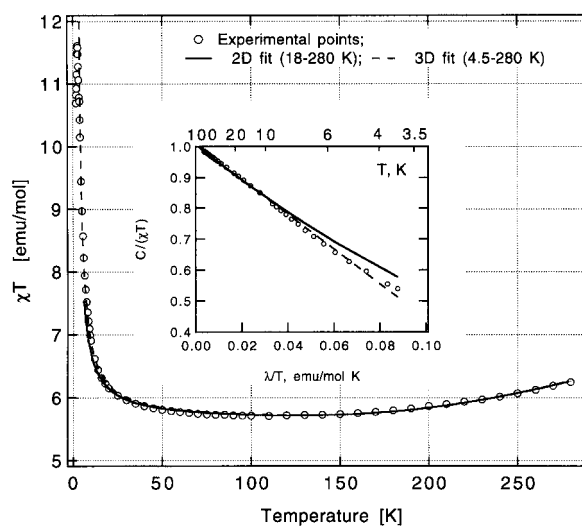


Figure 1. The temperature dependence of $\chi_m T$ for the 2D complex $\{\text{Mn}(\text{hfac})_2\}_3(\mathbf{3R}_\Delta)_2 \cdot n\text{-C}_7\text{H}_{16}$. Open circles are the experimental data, the solid and the dashed lines are the least squares fits for a 2D and 3D lattice, respectively. The inset shows the details of the low temperature behavior in the $C/\chi T$ versus λ/T form.

V-G Mn(II)-Induced Formation of a [3+3] Benzene Dimer Derivatives

A number of studies have been conducted on the dimerization of aromatic compounds. Most of these compounds are formed by a Diels-Alder-type cycloaddition reaction, *i.e.* [2+2] or [2+4]. We found a unique aromatic [3+3] cycloaddition in the presence of $\text{Mn}(\text{II})$ ion. In the course of our study of self-assembly of magnetic metal ions and bis- and tris(aminoxyl) radicals described in V-F, we found the formation of a unique [3+3] benzene dimer structure as a side reaction. Some reports have described the [3+3] cycloaddition of organic molecules but not of aromatic compound. Our crystallographic characterization would help shed light on the mechanistic detail of Lewis acid-catalysed cycloaddition and free-radical reactions.

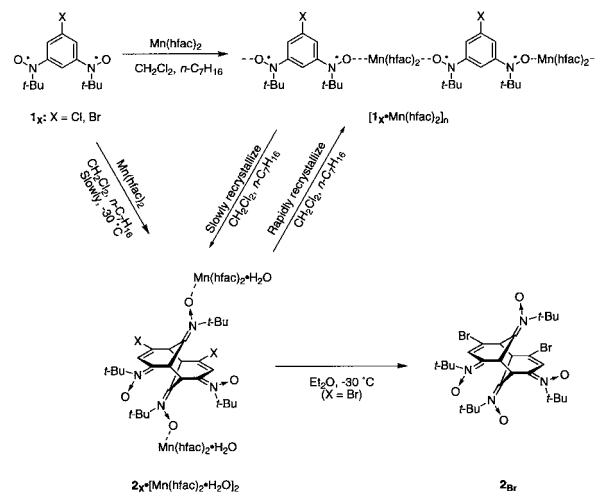
V-G-1 Mn(II)-Induced Formation and Structural Elucidation of a [3+3] Benzene Dimer Derivative from *m*-Phenylenebis(*N*-*tert*-butylaminoxyl)

IWAHORI, Fumiyasu¹; INOUE, Katsuya; IWAMURA, Hiizu²
(¹GUAS; ²Kyushu Univ.)

[*J. Am. Chem. Soc.* **121**, 7264 (1999)]

One-dimensional ferrimagnetic complexes, $[\text{Mn}(\text{hfac})_2 \cdot \mathbf{1}_X]_n$ ($X = \text{Cl}$ or Br), are typically obtained by the reaction of $\text{Mn}(\text{hfac})_2$ with $\mathbf{1}_X$. When it takes a few days for crystallization, however, black solutions often turn yellow in about one day and yellow crystalline precipitates are obtained. A solution of $\mathbf{1}_{\text{Br}}$ in CH_2Cl_2 was added to a suspension of $\text{Mn}(\text{hfac})_2$ in *n*- C_7H_{16} at 0 °C and the mixture was stored at -30 °C. After a few days, yellow needles of $\mathbf{2}_{\text{Br}} \cdot [\text{Mn}(\text{hfac})_2 \cdot \text{H}_2\text{O}]_2 \text{CH}_2\text{Cl}_2$ were obtained (85.2%). An X-ray structure analysis revealed that $\mathbf{2}_X \cdot [\text{Mn}(\text{hfac})_2 \cdot \text{H}_2\text{O}]_2 \text{CH}_2\text{Cl}_2$ has a [3+3] benzene-dimer structure $\{X = \text{Cl}$ or Br ; $\mathbf{2}_X = 3,10$ -dihalo-5,8,11,12-tetrakis(*N*-*tert*-butylimino)-tricyclo[5,3,1,1^{2,6}]dodeca-3,9-diene *N,N',N'',N'''*-tetraoxide}. When $\mathbf{2}_{\text{Br}} \cdot [\text{Mn}(\text{hfac})_2 \cdot \text{H}_2\text{O}]_2 \text{CH}_2\text{Cl}_2$ was dissolved in Et_2O and the solution was stored at -30 °C, white powder of $\mathbf{2}_{\text{Br}} \cdot 2\text{H}_2\text{O}$ free of $\text{Mn}(\text{hfac})_2$ precipitat-

ed out in 30 minutes (68.8%). Spectroscopic data on $\mathbf{2}_{\text{Br}}$ are in good agreement with its structure. The spectra of $\mathbf{2}_{\text{Br}}$ in CH_2Cl_2 is time-dependent and converted eventually to that of monomeric biradical $\mathbf{1}_{\text{Br}}$ by showing four isosbestic points. The result indicates that the dissociation process of $\mathbf{2}_{\text{Br}}$ into two molecules of $\mathbf{1}_{\text{Br}}$ is very clean.



Scheme 1. Transverse scheme between [3+3] benzene derivatives and ID ferrimagnetic complexes.

V-H Synthesis of Chiral Molecule-Based Magnets

There is a phenomenological resemblance between natural and magnetic optical activity. The former is due to the handedness of molecular structure, whereas the latter is due to the magnetic field-induced circular dichroism. In 1984 Barron and Vrbancich call “magneto-chiral dichroism” (MChD) for a link between two phenomena. In 1997, Rikken and Raupach observed the MChD effect of tris(3-trifluoroacetyl- \pm -camphorato)europium (III) in the paramagnetic state. However, the MChD effect in the paramagnetic state is small. It's important to make the fully chiral molecule-based magnets, which expected to be strong MChD effect. There are still no examples of molecule-based chiral magnet. Novel properties are expected for such compounds.

The design of molecular materials with interesting electrical and/or magnetic properties is one of the major challenges of science in the last few years. It's possible to modify the molecular structure in the molecule-based magnetic materials. Recently, we introduced a strategy of using π -conjugated polyaminoxyl radicals with high-spin ground states as bridging ligands for magnetic metal ions in order to assemble and align the electron spins on a macroscopic scale. The crystal structures of these complexes are known, and some cases, the magnetic structures are analyzed. The dimensionality of the complex and the sign and magnitude of the exchange coupling between the neighboring spins may be readily tuned by this strategy. When we use a bidentate bisaminoxyl radicals as ligand and manganese(II) hexafluoroacetylacetonate, $\text{Mn}(\text{II})(\text{hfac})_2$, we can make one-dimensional complexes. If we use chiral triplet bisaminoxyl radicals for the construction of one-dimensional magnet, we can expect to make chiral molecule-based magnets.

V-H-1 A Chiral Molecule-based Metamagnet Made by a Chiral Triplet Organic Radical and Manganese Ion

KUMAGAI, Hitoshi; INOUE, Katsuya

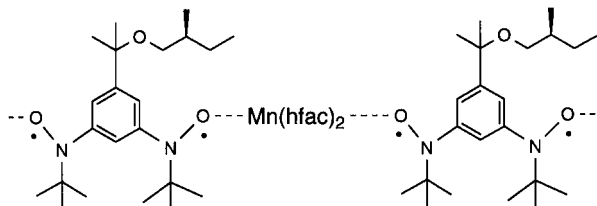
[*Angew. Chem., Int. Ed. Engl.* **38**, 1601 (1999).]

The chiral biradical, 1,3-bis(*N*-*tert*-butylamino-*N*-oxyl)-5-[1'-methyl-1'-{(S)-2''-methylbutoxy}]-ethylbenzene ($\mathbf{1}$) was prepared and was mixed with an equimolar amount of dehydrated $\text{Mn}(\text{hfac})_2$ in diethyl ether/*n*-heptane and the mixture was evaporated. Deep brown block crystals were obtained in 1 day at -30 °C.

X-ray crystal structure analysis of the complex revealed the formation of a one-dimensional structure. (Scheme 1) The oxygen atoms of the terminal aminoxyl radicals of biradical $\mathbf{1}$ are ligated to two different manganese ions in *trans* position to form a one-dimensional helical chain along the *c* crystal axis. The bisaminoxylbenzene unit is in a chiral conformation and forms a (*R*)-helical structure.

The magnetization at 1.8 K revealed metamagnetic behavior (Figure 1); while the response of the magnetization was not sensitive to the weak applied magnetic field below *ca.* 500 Oe, a behavior characteristic of an antiferromagnet. A sharp rise and approach to saturation of magnetization characteristic of a ferromagnet was

observed at higher applied magnetic field. A saturation magnetization value of *ca.* $2.7 \mu_B$ was reached at 1.8 K at 3 Tesla, which suggests the antiferromagnetic coupling between the manganese(II) ion and **1**.



Scheme 1. Polymeric chain structure of $[1 \cdot \text{Mn}(\text{hfac})_2]_n$.

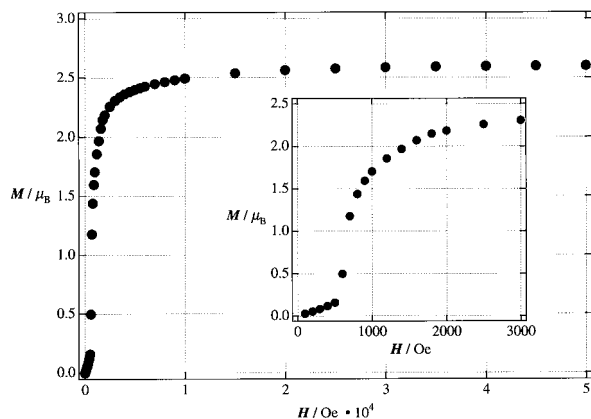


Figure 1. Field dependencies of the magnetic moment of a polycrystalline sample of $[1 \cdot \text{Mn}^{\text{II}}(\text{hfac})_2]_n$ at 1.8 K. Inset shows magnetic field range of 0 to 3000 Oe.

V-H-2 Synthesis and Characterization of a Novel Chiral Molecular-based Ferrimagnet Prepared from a Chiral Nitronyl Nitroxide Radical and Manganese(II) Ion

KUMAGAI, Hitoshi; INOUE, Katsuya

The chiral radical **2** was synthesized and was mixed with an equimolar amount of dehydrated $\text{Mn}(\text{hfac})_2$ in diethyl ether/*n*-heptane and the mixture was evaporated to *ca.* 10 ml. Green block crystals were obtained at -30°C in 1 week.

The X-ray crystal structure analysis revealed that both crystals of **2** and complex $[2 \cdot \text{Mn}^{\text{II}}(\text{hfac})_2]_n$ belongs to the same chiral space group $P2_12_12_1$ (No. 19). The molecular structure of $[2 \cdot \text{Mn}^{\text{II}}(\text{hfac})_2]_n$ is depicted in Figure 1. One-dimensional chain elongates along the crystal *a*-axis. The radicals are bound to the Mn(II) ion in cis-coordination to each other. In this complex, the metal center exhibits the all Δ configuration. Because of the use of the chiral ligand, the complex crystallized in chiral space group and no Λ chirality of the Mn(II) are existed in this crystal. Since no inversion centers are present in this space group, chains are isotactic as all units and the crystal lattice as a whole is chiral.

Magnetization measurements have been performed at 2 K. The magnetization increases very rapidly, and reaches a plateau about 3.6 B.M. at 1.5 T. This value suggests the antiferromagnetic coupling between the manganese(II) ion and **2** (Theoretical value is 4 B.M. ($5/2 - 1/2 = 4/2$.) AC susceptibility measurements revealed that $[2 \cdot \text{Mn}^{\text{II}}(\text{hfac})_2]_n$ behaves as ferrimagnet below 4.5 K. The existence of weak ferromagnetic interchain interaction is suggested.

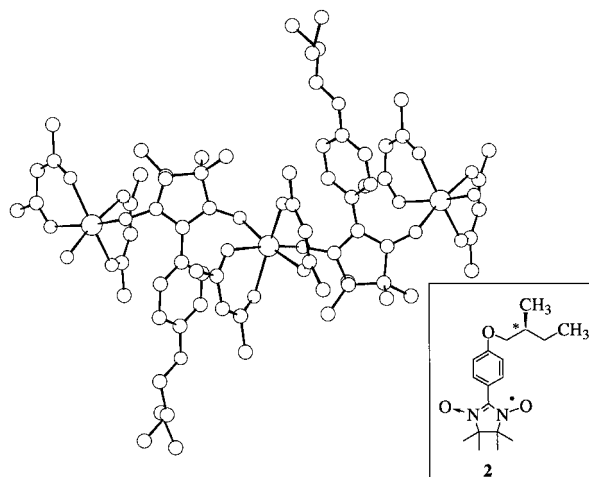


Figure 1. View of a helical chain formed by chiral nitronyl nitroxide **2** and $\text{Mn}(\text{II})(\text{hfac})_2$. Hydrogen atoms and fluorine atoms are omitted for clarity

V-I Synthesis and Characterization of Quantum-Spin Systems

Quantum spin systems have been much attracted for several decades. Haldane's conjecture in 1983 on the difference between a Heisenberg antiferromagnetic chain of integer-spin magnitude and that of half-integer-spin magnitude called renewed interest. The properties of $S = 1$ spin chain with a finite energy gap between the ground state and excited states have been extensively studied both theoretically and experimentally. Then, interested is the crossover between the dimer state and Haldane state, for example, in the $S = 1/2$ alternating chain with ferromagnetic and antiferromagnetic interactions. We have designed and synthesized two types of $S = 1/2$ chains with ferromagnetic and antiferromagnetic interactions. Moreover, we made a two-dimensional antiferromagnetic lattice of the ferromagnetic spin pairs. Another topic is the double chain systems, which is interesting from the aspect of the Haldane state and high T_C superconductivity. We designed and synthesized a railroad trestle compound and observed the existence of an energy gap above the singlet ground state.

V-I-1 Magnetic Properties of Low Dimensional Quantum Spin Systems Made of Stable Organic Biradicals PNNNO, F₂PNNNO and PIMNO

HOSOKOSHI, Yuko; NAKAZAWA, Yasuhiro; INOUE, Katsuya; TAKIZAWA, Kohichi¹; NAKANO, Hiroki¹; TAKAHASHI, Minoru¹; GOTO, Tsuneaki¹
(¹ISSP, Univ. Tokyo)

[Phys. Rev. B in press]

Stable organic biradical crystals PNNNO, F₂PNNNO and PIMNO of the PNNNO family were synthesized. (PNNNO = 2-[4'-(*N*-*tert*-butyl-*N*-oxyamino)phenyl]-4,4,5,5-tetramethyl-4,5-dihydro-1*H*-imidazol-1-oxyl 3-oxide, F₂PNNNO = 2-[2',6'-difluoro-4'-(*N*-*tert*-butyl-*N*-oxyamino)phenyl]-4,4,5,5-tetramethyl-4,5-dihydro-1*H*-imidazol-1-oxyl 3-oxide, PIMNO = 2-[4'-(*N*-*tert*-butyl-*N*-oxyamino)-phenyl]-4,4,5,5-tetramethyl-4,5-dihydro-1*H*-imidazol-1-oxyl) PNNNO and PIMNO crystallize to form quasi-one-dimensional lattices, but F₂PNNNO to form a quasi-two-dimensional lattice. The temperature dependences of the susceptibility and the high-field magnetization process up to 34 T were measured down to 0.5 K. The results are analysed by comparing with the theoretical calculations based on the crystal structures. PNNNO and PIMNO are considered to be antiferromagnetic Heisenberg spin chains consisting of $S = 1/2$ spin pairs (dimers) in which the two spins are coupled ferromagnetically. Both compounds undergo antiferromagnetic phase transitions at 1.1 and 2.5 K, respectively due to weak interchain interactions. The three-dimensional nature of the transition is examined by the thermodynamic discussion through specific heat measurements. On the other hand, F₂PNNNO is thought to be a two-dimensional Heisenberg system, in which the spin pairs are connected by two types of antiferromagnetic interactions. The magnetism of F₂PNNNO is characterized by the singlet ground state and a plateau in the magnetization isotherm.

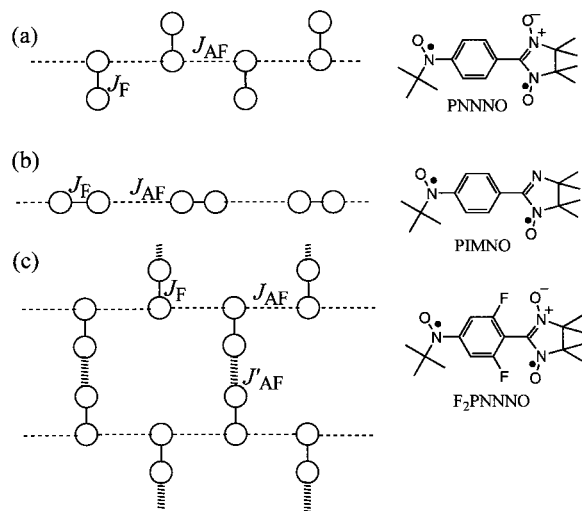


Figure 1. Scheme of the magnetic interactions in (a) PNNNO, (b) PIMNO and (c) F₂PNNNO with their molecular structures.

V-I-2 Construction of a Quantum-Spin System of $S = 1/2$ Antiferromagnetic Chain with the Next-Nearest-Neighbor Interactions

HOSOKOSHI, Yuko; KATOH, Keiichi¹; INOUE, Katsuya; GOTO, Tsuneaki¹
(¹ISSP, Univ. Tokyo)

[J. Phys. Soc. Jpn. **68**, 2910 (1999)]

We have succeeded in synthesizing a new compound with a railroad trestle structure, *i.e.*, a zigzag chain with next-nearest-neighbor interactions. We have newly synthesized organic radicals F₂PIMNH and Cl₂PIMNH, where F₂PIMNH = 2-[4'-*N*-*tert*-butylamino-2',6'-difluorophenyl]-4,4,5,5-tetramethyl-4,5-dihydro-1*H*-imidazol-1-oxyl and Cl₂PIMNH = 2-[4'-*N*-*tert*-butylamino-2',6'-dichlorophenyl]-4,4,5,5-tetramethyl-4,5-dihydro-1*H*-imidazol-1-oxyl. Both crystals include zigzag uniform chains made of hydrogen bondings. The magnetism of Cl₂PIMNH is explained by the Heisenberg antiferromagnetic uniform chain model with $2J/k_B = -3.6$ K and gapless ground state is suggested. On the other hand, static magnetic measurements of F₂PIMNH suggest the nonmagnetic ground state and the existence of a finite gap in its excitation spectrum. In this crystal, the next-nearest-neighbor contacts are seen, which are believed to be the origin of the energy gap.

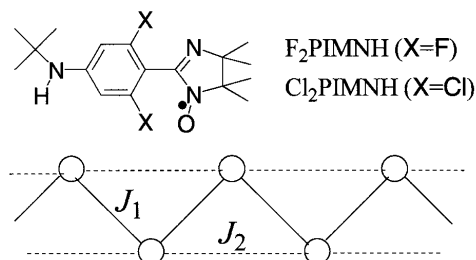


Figure 1. Scheme of the magnetic interactions in F₂PIMNH. Uniform chain with the next nearest neighbor interactions.

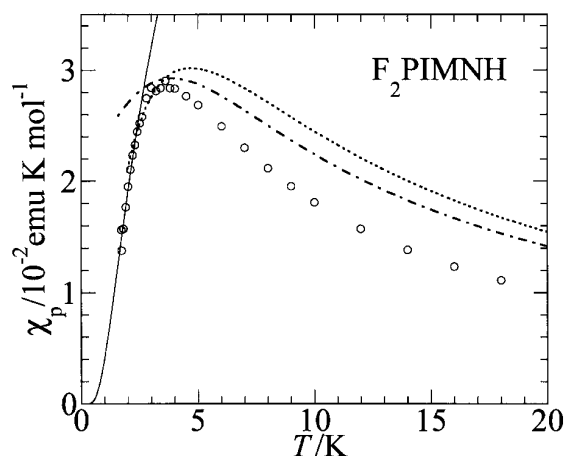


Figure 2. (a) Temperature dependence of χ_p of F₂PIMNH. The solid curve is the fit of $\chi \propto \exp\{-\Delta/T\}$ with $\Delta = 3.1$ K. The dotted broken curve is the calculation for the uniform chain with $2J/k_B = -6$ K, the interchain interactions by the mean-field treatment of $2zJ'/k_B = -5.2$ K are adopted. The dotted curve represents the calculation for the alternating chain with $2J_1/k_B = -7.9$ K and $2J_2/k_B = -6.3$ K.

V-J Pressure Effects on Magnetic Materials

“Pressure” is a powerful tool to control the molecular packings and physical properties. The molecule-based materials with small densities are “soft” and can be expected to exhibit large pressure effects. For the magnetic measurements with high-accuracy, we have developed a small high-pressure clamp cell made of Cu-Ti alloy which can be equipped to a Quantum Design SQUID magnetometer for the dc and ac magnetic measurements. The inner pressure of the clamp cell has been calibrated by the superconducting transition temperature of Pb. The maximum pressure maintained is *ca.* 7 kbar, the reproducibility is good, and the temperature variation of pressure in the cell is within *ca.* 0.3 kbar.

We study the pressure effects on the molecule-based chain compounds. We have observed the pressure-induced phenomena of (1) crossover from an alternating chain to a uniform chain, (2) dimensional-crossover from 2D to 1D, and (3) change of the sign of the interchain interactions. We also apply the pressure to some intermetallic compounds which show large volume effects.

V-J-1 Pressure-Induced Crossover from Alternating to Uniform Interaction in an $S = 1/2$ One-Dimensional Heisenberg Antiferromagnet

MITO, Masaki¹; KAWAE, Tatsuya¹; HOSOKOSHI, Yuko; INOUE, Katsuya; KINOSHITA, Minoru²; TAKEDA, Kazuyoshi¹
(¹Kyushu Univ.; ²Sci. Univ. Tokyo in Yamaguchi)

[*Solid State Commun.* **111**, 607 (1999)]

We have confirmed the pressure-induced crossover from the alternating to the uniform one-dimensional (1D) spin system in an organic compound as a function of applied pressure (p) by the measurements of heat capacity. The pentafluorophenyl nitronyl nitroxide radical (F₅PNN), which is the 1D alternating Heisenberg antiferromagnet of spin $S = 1/2$ with $\alpha = J_2/J_1 \sim 0.4$ at ambient pressure, has transformed into the uniform one ($\alpha = 1$) at $p = 6.5$ kbar. This pressure induced crossover was made clear by observing the change of initial gradient of heat capacity, which transformed from exponential to linear at low temperature. The crystal structure of F₅PNN at the room temperature and ambient pressure is of the uniform spin chain, and the pressure must play the role of suppressing the structural transition into the alternating system.

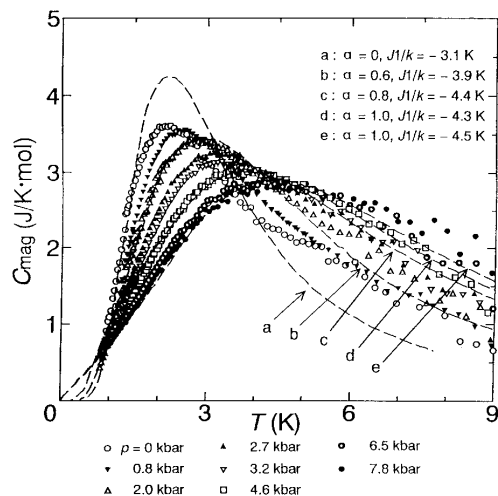


Figure 1. Temperature dependence of C_{mag} of F₅PNN under the pressure up to 7.8 kbar. The broken lines (a-e) express Duffy *et al.*'s theoretical curves of C_{mag} up to 7.8 kbar with such two parameters as α and J_1/k_B .

V-J-2 Pressure Effects on Organic Radicals with Ferromagnetic and Antiferromagnetic Interactions

HOSOKOSHI, Yuko; INOUE, Katsuya

[*Synth. Met.* **103**, 2323 (1999)]

Magnetic properties of stable organic biradicals under pressure are presented. The dimensional crossover from two-dimension to one-dimension is induced by pressure in F₂PNNNO, whereas the properties of the corresponding one-dimensional material, PNNNO is almost independent of the pressure. The phase transition temperature of the quasi-one-dimensional antiferromagnet, PIMNO become higher with applied pressure. The increase of the interchain interactions by pressurization has been observed, whereas the intrachain interactions are almost independent of the pressure.

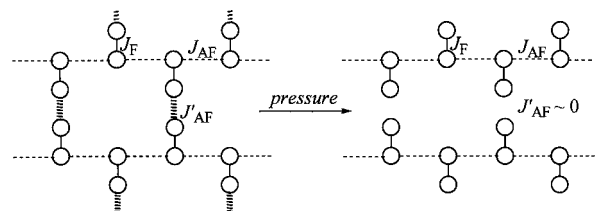


Figure 1. Scheme of the magnetic interactions in F₂PNNNO. Pressure-induced dimensional crossover from 2D to 1D.

V-J-3 Pressure Effect on Mn Complexes of Bisaminoxyl Radicals

HOSOKOSHI, Yuko; SUZUKI, Kentaro¹; INOUE, Katsuya; IWAMURA, Hiizu²
(¹GUAS; ²Kyushu Univ.)

[*Mol. Cryst. Liq. Cryst.* in press]

The pressure effects on magnetic properties of one-dimensional Mn complexes with 1,3-bis(*N-tert*-butylaminoxyl)benzene and 5-chloro-1,3-bis(*N-tert*-butylaminoxyl)benzene have been studied. These complexes have weak interchain interactions with different signs and the former is a metamagnet and the latter is a ferrimagnet at ambient pressure. The interchain interactions of the former is enhanced by pressurization. The transition temperature becomes higher and the critical

field becomes larger with applying pressure. The closer spacing of each chains caused by pressurization, yields larger antiferromagnetic interchain interactions in this compound.

On the other hand, the response to the pressure of the latter ferrimagnet, is rather complicated. The transition temperature becomes higher and the antiferromagnetic interchain interactions are induced by pressurization. The interchain exchange coupling in this compound should be sensitive to the relative orientation of the chain structure. The decrease of the ferromagnetic contribution and/or the increase of the antiferromagnetic one in the interchain interactions is brought about by pressurization.

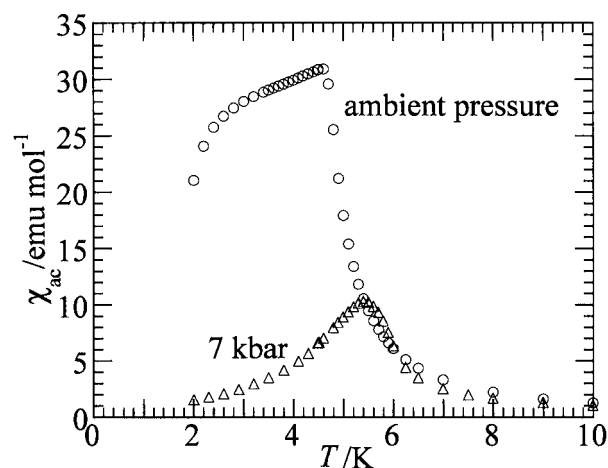


Figure 1. Temperature dependence of the ac susceptibilities of $[\text{Mn}(\text{hfac})_2] \cdot \{5\text{-chloro-1,3-bis}(N\text{-tert-butylaminoxyl})\text{benzene}\}$ at ambient pressure and under 7 kbar.

V-J-4 The Magnetic Phase Diagram and Pressure Effect on the Magnetic Properties of the $\text{Y}_{1-x}\text{Gd}_x\text{Mn}_2$ Intermetallic Compounds

DUBENKO, Igor S.¹; GAIDUKOVA, Irina Yu.²; HOSOKOSHI, Yuko; INOUE, Katsuya; MARKOSYAN, Ashot S.^{2,3}

(¹Moscow Inst. Radioeng. Electron. Autom.; ²M. V. Lomonosov Moscow State Univ.; ³IMS)

[*J. Phys.: Condens. Matter* **11**, 2937 (1999)]

Magnetization up to 50 kOe, magnetic susceptibility under external pressure up to 5 kbar and thermal expansion of the cubic Laves phase compounds $\text{Y}_{1-x}\text{Gd}_x\text{Mn}_2$ were studied in a wide temperature range. Two well defined concentration regions were isolated in the x - T phase diagram: $0 \leq x < 0.2$, in which the antiferromagnetic structure is primarily determined by the d-d interaction (YMn₂-type), and $0.2 < x \leq 1$, in which the f-d interaction plays a dominant role (GdMn₂-type). It is concluded that both the Gd and Mn sublattices are ordered in GdMn₂ below $T_N = 108$ K, the change in the magnetic characteristics at 40 K interpreted as an antiferromagnetism – non-collinear ferrimagnetism transition. The intermediate $\text{Y}_{0.8}\text{Gd}_{0.2}\text{Mn}_2$ compound shows a freezing and time dependent effects at low temperatures characteristic for short range order. The effects can also be induced by external pressure at

higher Gd concentrations.

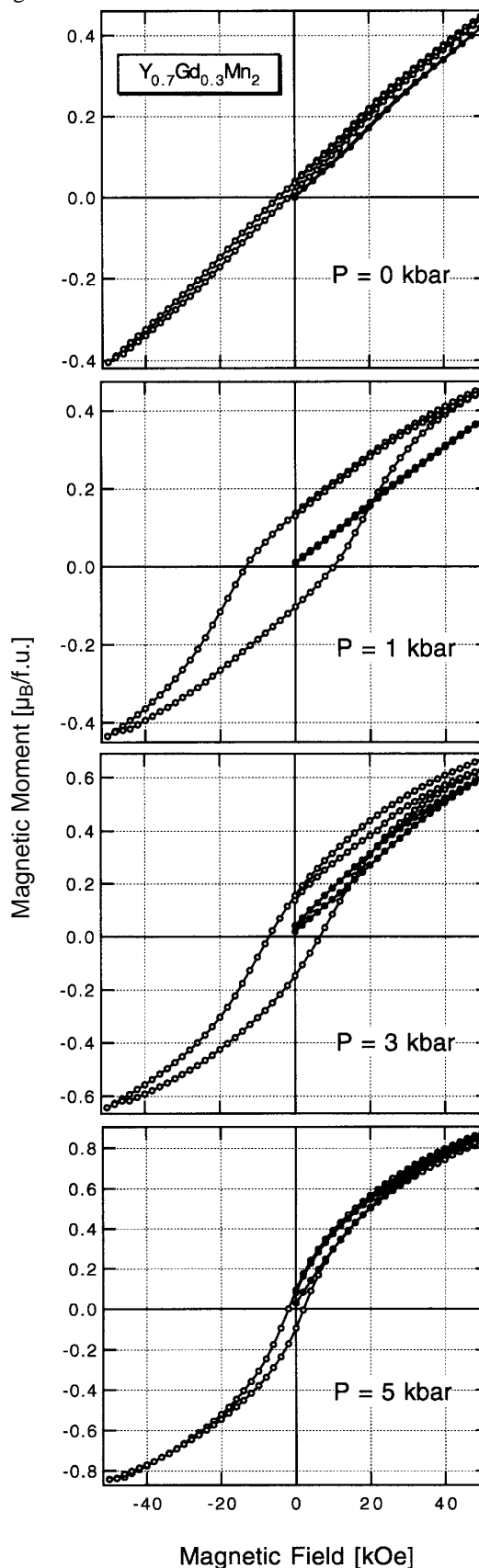


Figure 1. The hysteresis loops of $\text{Y}_{0.7}\text{Gd}_{0.3}\text{Mn}_2$ at 4 K under pressures 0, 1, 3 and 5 kbar. Full and open symbols correspond to the z.f.c. and f.c. (50 kOe) sample, respectively.

V-J-5 Concentration and Pressure Dependence of the Magnetic Ordering in the $Y(Mn_{1-x}Me_x)_2$ Compounds with Me = Al, Fe and Ni

DUBENKO, Igor S.¹; GAIDUKOVA, Irina Yu²; HOSOKOSHI, Yuko; INOUE, Katsuya; MARKOSYAN, Ashot S.^{2,3}

(¹Moscow Inst. Radioengin. Electron. Autom.; ²M. V. Lomonosov Moscow State Univ.; ³IMS)

[*J. Magn. Magn. Mater.* **195**, 687 (1999)]

Magnetic susceptibility of the $Y(Mn_{1-x}Me_x)_2$ (Me = Al, Fe and Ni) compounds was measured in the temperature range 2 ÷ 400 K under external pressure up to 5 kbar. The role of the interatomic Mn-Mn spacing in stabilising the antiferromagnetic transformed phase has been revealed. The value of $\partial T_N/\partial P \approx -50$ K/kbar was found essentially higher than in the mother compound YMn_2 . A freezing effect was observed in the non-transformed phase which was related to the break-down of the quantum spin liquid state.

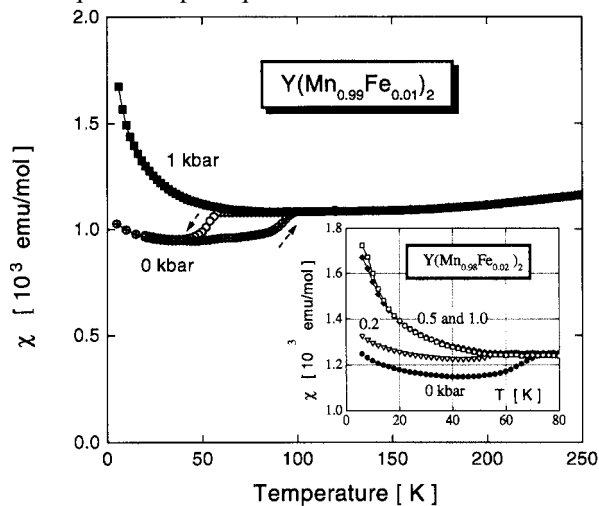


Figure 1. The temperature dependence of χ_{DC} for $Y(Mn_{0.99}Fe_{0.01})_2$ at 1 kbar and ambient pressure. The inset shows the variation of χ_{DC} vs. T on cooling for $Y(Mn_{0.98}Fe_{0.02})_2$ at different pressures.

V-K Desorption Induced by Electronic Transitions at the Surface of van der Waals Condensates

The electronic excitation on the surface of a van der Waals condensate may lead the desorption of neutral and charged molecules, either in the ground state or in excited ones. The phenomena discussed here are neither thermal desorption nor direct mechanical sputtering but processes through a transformation of an electronic excitation energy into a kinetic energy of a desorbing particle. Close investigation of this DIET (Desorption Induced by Electronic Transitions) phenomena will reveal the dynamical aspect of the electronic excitation and its relaxation process at the surface. In this research project, we have determined the absolute total desorption yield at the surface of solid Ne and have investigated the desorption of the excimer, Ne₂*.

V-K-1 Absolute Measurement of Total Photo Desorption Yield of Solid Ne in Vacuum Ultraviolet Range

[to be submitted]

ARAKAWA, Ichiro^{1,2}; ADACHI, Takashi²; HIRAYAMA, Takato²; SAKURAI, Makoto³
(¹IMS; ²Gakushuin Univ.; ³Kobe Univ.)

[Surf. Sci. submitted]

Absolute yields of photo-induced desorption at the surface of solid Ne have been measured between 25 and 100 nm of wavelength of incident light. There are strong dependence of the total desorption yield of Ne both on the excitation energy and on the thickness of Ne films. On a thick film, the desorption yield is 1–2 atoms/photon by the bulk exciton excitation and 2–10 atoms/photon by the bulk ionization. The main component in the desorbed species is neutral Ne molecules in the ground state; the absolute yield of metastable desorption at the excitonic excitation is the order of 10⁻³ metastable/photon.¹⁾ The absolute yield of the order of unity for the total desorption by the bulk exciton excitation can quantitatively be understood by the following internal sputtering model. From optical absorption data, the number of excitons created per photon per layer is estimated at about 0.1. The kinetic energies of the particles desorbed through the cavity ejection mechanism is about 0.2 eV and those by the excimer dissociation one 1 eV. Because the cohesive energy of Ne is 0.019 eV, the desorbing particle, which is originated from the 2nd or 3rd layer, can blow 10 or more neutral Ne atoms in the overlayer off. The product of these values results in an order of unity of absolute yield of the total desorption. By the surface exciton excitation, the yield is 0.1–0.3 atoms/photon, which value means that the desorption probability of the surface exciton is almost unity.

Reference

- 1) T. Hirayama, A. Hayama, T. Koike, T. Kuninobu, I. Arakawa, K. Mitsuke, M. Sakurai and E. V. Savchenko, *Surf. Sci.* **390**, 266 (1997).

V-K-2 Desorption of an Excimer from the Surface of Solid Ne by Low Energy Electron or Photon Impact

HIRAYAMA, Takato¹; HAYAMA, Akira¹; ADACHI, Takashi¹; ARAKAWA, Ichiro^{1,2}; SAKURAI, Makoto³
(¹Gakushuin Univ.; ²IMS; ³Kobe Univ.)

Desorption of excited dimers Ne₂* in ³Σ_u state from the surface of solid Ne initiated by the creation of a valence exciton was confirmed experimentally using low energy electron or monochromatic VUV light as excitation sources. The kinetic energy of desorbed excimer (Ne₂* ³Σ_u) was (0.2 ± 0.1) eV, which is consistent with a recent quantum mechanical calculation.¹⁾ It is found that the vibrational relaxation of a molecular type exciton is a slow process compared to the time scale of desorption. Desorption of excimers at the excitation of the first order surface exciton was found to be inefficient compared to that by the creation of bulk excitons, which is in striking contrast to the case of the excited atom desorption. The mechanism of excimer desorption can be explained by a cavity ejection model as in the atomic desorption case.

Reference

- 1) L. F. Chen, G. Q. Huang and K. S. Song, *Nucl. Instrum. Methods Phys. Res., Sect. B* **116**, 61 (1996).

V-L Synthesis and Physical Properties of Novel Molecular Metals

Development of organic materials which exhibit interesting electrical properties such as metallic conductivity and superconductivity has received considerable attention. A bis-fused TTF, 2,5-bis(1,3-dithiol-2-ylidene)-1,3,4,6-tetrathiapentalene (TTP) is a promising π -electron framework for preparation of stable metals down to low temperatures, because it has a ladder-like array of sulfur atoms indispensable for constructing two-dimensional network of the donors. In fact, we have found that the unsubstituted TTP has a strong tendency to afford highly conducting radical cation salts retaining metallic conductivity down to ≤ 1.2 K regardless of shape and size of counter anions. In the present study, we have developed several organic metals by means of comprehensive modification of TTP, namely i) introduction of substituents, ii) exchange of sulfur atoms in the TTP framework with selenium, iii) synthesis of TTP analogs possessing non-TTF donor unit.

V-L-1 (CPDT-STF)(TCNQ): A New Charge-Transfer Complex Metallic Down to Low Temperature

TANIGUCHI, Masateru¹; MISAKI, Yohji^{1,2}; TANAKA, Kazuyoshi¹; YAMABE, Tokio¹; MURATA, Kyoji³; MORI, Takehiko³

(¹Kyoto Univ.; ²IMS; ³Tokyo Inst. Tech.)

[*Solid State Commun.* **111**, 559 (1999)]

A new charge transfer complex (CPDT-STF)-(TCNQ) has been prepared. An X-ray crystal structure analysis revealed that this complex is composed of the donor and acceptor sheets orthogonally arranged to each other (Figure 1), which is similar to (ET)(TCNQ) and (ET)(TCNQF₄). The band calculations indicate that the CPDT-STF layer has significantly two-dimensional interaction, while the TCNQ one has one-dimensional Fermi surface. The electrical resistivity of the present complex showed metallic temperature dependence down to 0.6 K. The thermoelectric power was negative and changed from the positive to the negative gradient at 60 K. The static magnetic susceptibility and transport properties indicate coexistence of local and itinerant electrons in the present complex.

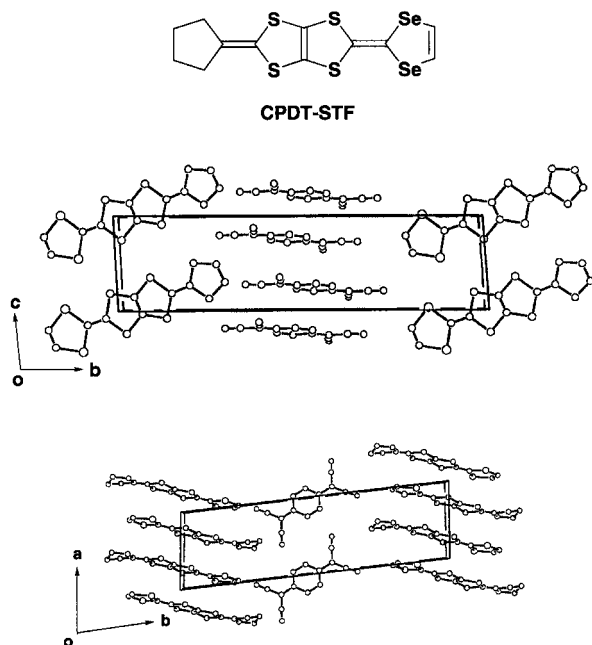


Figure 1. Crystal structure of (CPDT-STF)(TCNQ).

V-L-2 Structures and Electrical Properties of (EO-TTP)₂AsF₆

MISAKI, Yohji^{1,2}; TANAKA, Koji¹; TANIGUCHI, Masateru¹; YAMABE, Tokio¹; KAWAMOTO, Tadashi³; MORI, Takehiko³

(¹Kyoto Univ.; ²IMS; ³Tokyo Inst. Tech.)

Tetrahedral and octahedral anions based on EO-TTP, where EO-TTP is 2-(4,5-ethylenedioxy-1,3-dithiol-2-ylidene)-5-(1,3-dithiol-2-ylidene)-1,3,4,6-tetrathiapentalene, afforded radical cation salts retaining metallic conductivity down to low temperature (1.5–4.2 K). X-Ray structure analysis of the AsF₆ salt (EO-TTP)₂AsF₆ reveals that it has the so-called b-type array of donors (Figure 1). A tight binding band calculation suggested that this salt has a two-dimensional closed Fermi surface.

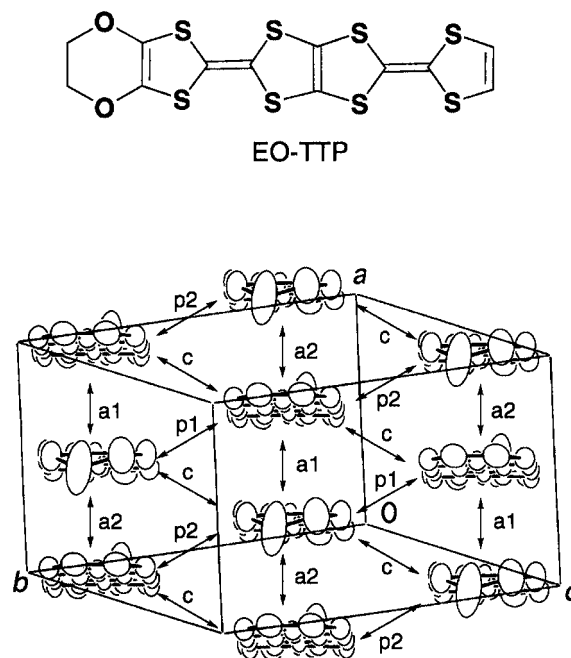


Figure 1. Donor sheet structure of (EO-TTP)₂AsF₆; The intermolecular overlap integrals are $a_1 = 26.9$, $a_2 = 25.2$, $p_1 = 0.47$, $p_2 = 0.11$, $c = -9.07 \times 10^{-3}$.

V-L-3 A Quasi Three-Dimensional Organic Conductor Based on a TTP Analogue Containing Thiopyran-4-ylidene

MISAKI, Yohji^{1,2}; KAIBUKI, Tadahiro¹; TANIGUCHI, Masateru¹; TANAKA, Kazuyoshi¹; TAKIMIYA, Kazuo³; MORIKAMI, Atsushi³; OTSUBO, Tetsuo³; MORI, Takehiko⁴

(¹Kyoto Univ.; ²IMS; ³Hiroshima Univ.; ⁴Tokyo Inst. Tech.)

We have demonstrated that a bis-fused TTP, 2,5-bis-(1,3-dithiol-2-ylidene)-1,3,4,6-tetrathiapentalene (TTP) has afforded many metallic radical-cation salts stable down to liquid helium temperature regardless of shape and size of counter anions, in which the donors have a two-dimensional array. In contrast, (TM-TPDS)₂AsF₆, where TM-TPDS is 2-[4,5-bis(methylthio)-1,3-diselenol-2-ylidene]-5-(thiopyran-4-ylidene)-1,3,4,6-tetrathiapentalene has no two-dimensional conducting sheet in contrast to usual TTP conductors. The donors are arranged in a "windmill" manner in the *bc* plane (Figure 1). The anion is located on the center of "windmill," and are surrounded by methylthio groups in the donors. The donors are alternately stacked along the *a* axis. There are many sulfur-sulfur contacts shorter than the sum of van der Waals radii (3.70 Å) between the central tetrathiapentalene moiety and the thiopyrane ring or methylthio groups. Thanks to a relatively large atomic coefficient of the sulfur atom in the thiopyrane ring, which is comparable to those of the others in the 1,3-dithiole rings, the calculated overlap integrals of the intercolumn interaction are comparatively large of about 10% of the intracolumn one. As a result, the Fermi surface of the present salt is indeed one-dimensional, however, interactions in the *bc* plane is isotropical, namely this salt may be regarded to be a quasi three-dimensional metal. This salt showed high conductivity of 240 S cm⁻¹ at room temperature, and exhibited metal-like temperature dependence down to 100 K. Below this temperature, the resistivity gradually increased.

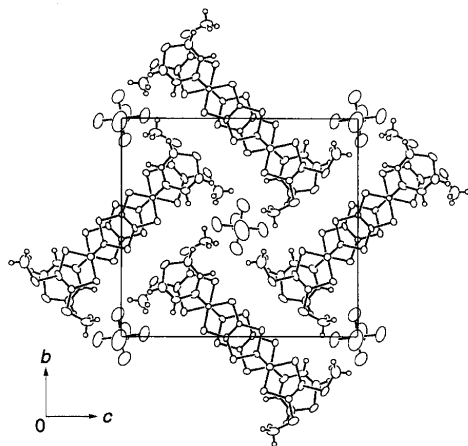
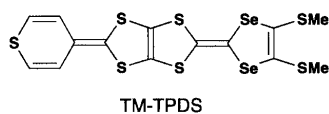


Figure 1. Crystal structure of (TM-TPDS)₂AsF₆.

V-L-4 Structures and Properties of Organic Metals Based on Dimethyl Substituted TTP Analogue

TANIGUCHI, Masateru¹; MISAKI, Yohji^{1,2}; TANAKA, Kazuyoshi¹; YAMABE, Tokio¹; MORI, Takehiko³

(¹Kyoto Univ.; ²IMS; ³Tokyo Inst. Tech.)

[*Synth. Met.* **102**, 1721 (1999)]

A selenium analogue of dimethyl substituted TTP (DM-TS-TTP) was prepared. (DM-TS-TTP)₂PF₆ showed metallic temperature dependence down to 4.2 K. X-Ray crystal structure analysis of this salt reveals that the donors form two-dimensional conducting sheets as is observed in most TTP type metals (Figure 1). The arrangement of donors is classified as the so-called β-type. The band structure calculated by a tight-binding method suggests that it has a quasi one-dimensional Fermi surface.

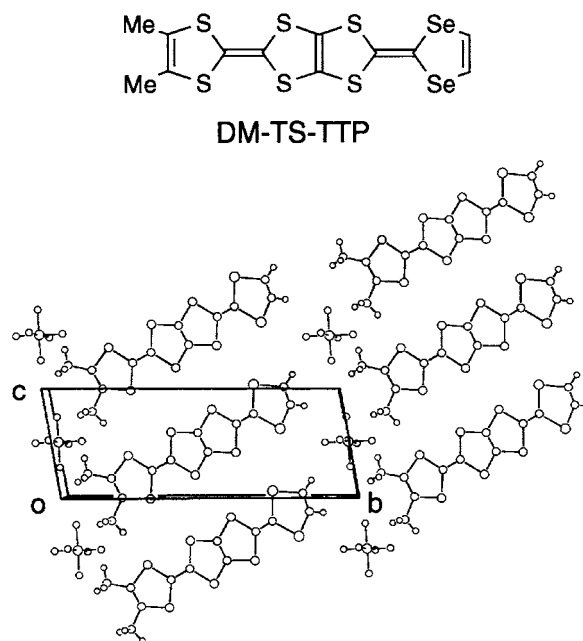


Figure 1. Crystal structure of (DM-TS-TTP)₂PF₆.

V-L-5 Synthesis and Properties of Methylthio Substituted ST-TTP Derivatives

MISAKI, Yohji^{1,2}; KAIBUKI, Tadahiro¹; MONOBE, Tae¹; TANAKA, Koji¹; TANIGUCHI, Masateru¹; TANAKA, Kazuyoshi¹; YAMABE, Tokio¹; TAKIMIYA, Kazuo³; MORIKAMI, Atsushi³; OTSUBO, Tetsuo³; MORI, Takehiko⁴

(¹Kyoto Univ.; ²IMS; ³Hiroshima Univ.; ⁴Tokyo Inst. Tech.)

[*Synth. Met.* **102**, 1781 (1999)]

A new ST-TTP donor TMEO-ST-TTP, where TMEO-ST-TTP is 2-[4,5-bis(methylthio)-1,3-diselenol-2-ylidene]-5-(4,5-ethylendioxy-1,3-dithiol-2-ylidene)-1,3,4,6-tetrathiapentalene, has been prepared. It affords highly conducting PF₆⁻ and AsF₆⁻ salts retaining

metallic conductivity down to 4.2 K, while the TCNQ complex and ClO_4^- salt are low conductive semi-conductors. X-Ray structure analyses reveal that (TMEO-ST-TTP)(TCNQ)(PhCl) has a DA type mixed stack, and that the donor array of (TMEO-ST-TTP)₂- ClO_4^- (DCE) in the conducting sheet resembles β -BEDT-TTF salts (Figure 1).

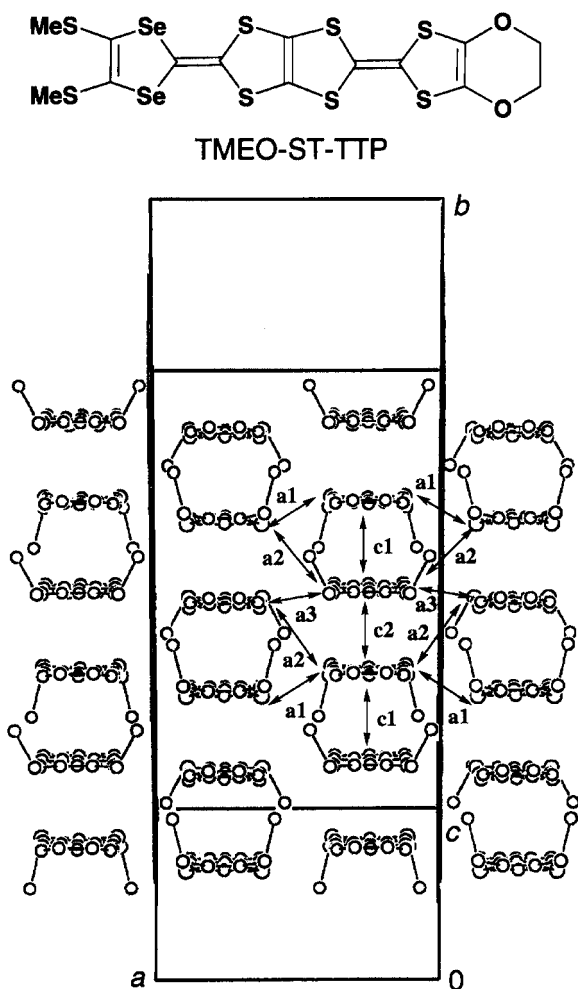


Figure 1. Donor sheet structure of (TMEO-ST-TTP)₂ClO₄⁻(DCE).

V-M Development of Model Core Potentials and Post Hartree-Fock Calculations to Atoms and Molecules

We have developed various types of model core potentials for various elements and applied the MCPs to investigate the electronic structures of atoms, molecules, and clusters at levels of post Hartree-Fock calculations.

V-M-1 Theoretical Study of Low-Lying Electronic States of TiCl and ZrCl

SAKAI, Yoshiko¹; MOGI, Kouichi¹; MIYOSHI, Eisaku
(¹Kyushu Univ.)

[*J. Chem. Phys.* **111**, 3989 (1999)]

Low-lying electronic states of TiCl and ZrCl were investigated by the complete active space SCF (CASSCF), multi-reference singly and doubly excited configuration interaction (MRSDCI), and multi-reference coupled pair approximation (MRCPA) calculations using the model core potential (MCP) method. The relativistic effects were incorporated in the MCP and basis sets for Zr at the level of Cowan and Griffin's quasirelativistic Hartree Fock method. The $^4\Phi$ state was found to be the ground state of TiCl whereas the $^2\Delta$ state was the ground state of ZrCl at all levels of calculations. Two low-lying excited states were very close in energy to the ground state. The excited $^4\Sigma^-$ and $^2\Delta$ states of TiCl were higher than the ground state by 0.102 eV and 0.458 eV, respectively, and the excited $^4\Phi$ and $^4\Sigma^-$ states of ZrCl were higher by 0.094 eV and 0.110 eV, respectively, at the MRCPA calculations.

V-M-2 Benchmarking of Model Core Potentials: Application to the Group 4 Metal Halogen Complexes (MX₄: M = Ti, Zr, Hf and X = F, Cl, Br, I)

DECKER, Stephan A.¹; KLOBUKOWSKI, Mariusz¹; SAKAI, Yoshiko²; MIYOSHI, Eisaku
(¹Univ. Alberta; ²Kyushu Univ.)

The reliability of the model core potential method was probed in a systematic study of the group 4 metal halogen complexes (MX₄; M = Ti, Zr, Hf and X = F, Cl, Br, I). In the first phase of the study we focused on the geometries of these tetrahedral complexes. The computed M-X distances were compared with experimental values, as well as those predicted using a variety of effective core potentials. The reaction energies for a

simple set of halogen diatomic substitution reactions of the MX₄ complexes leading to the mixed halogen complex, MX₂Y₂, were studied in the second part of this work. Although no experimental values are available for these reactions, comparison was again made with the values computed using a number of effective core potential methods. All of the calculations were carried out at the RHF and MP2 levels of theory. Discussion focuses on the predictability of the different pseudopotential techniques and the extent of the metal atom valence space. Furthermore, we comment on the importance of the metal atom valence basis set contraction scheme and polarization space.

V-M-3 Configuration Interaction Study of Differential Correlation Energies in Ca⁺, Ca and Ca⁻

OSANAI, You¹; NORO, Takeshi²; MIYOSHI, Eisaku
(¹Aomori Univ.; ²Hokkaido Univ.)

Configuration interaction (CI) calculations have been carried out for Ca⁺ (4s ²S, 3d ²D and 4p ²P^o), Ca (4s² ¹S and 3d4s ¹D) and Ca⁻ (4s²4p ²P^o) using very large Slate-type orbitals. The effect of Ar-like core was included by allowing the excitation from the most important subshells of the core, 3s and 3p, explicitly. A series of multi-reference single and double excitation CI calculations was performed adding important configurations representing valence correlation to the reference space, and convergence of CI energies and wavefunctions was investigated. Valence correlation can be described adequately only when the reference space is expanded so largely that valence correlation is almost completely described by reference functions alone. The relativistic effects were estimated by carrying out Dirac-Fock calculations. The present calculations gave the ionization potentials to 4s ²S, 3d ²D and 4p ²P^o to be 6.079, 7.819 and 9.179 eV, respectively, and the excitation energy to 3d4s ¹D to be 2.805 eV. All these calculated values are in good agreement with the observed values. The electron affinity was obtained to be 17.7 meV, which is in excellent agreement with the recent observed values, 17.5 ~ 21.5 meV.

V-N Theoretical Study of the Electronic Structures of Weakly Bound Molecules

The electronic structures of weakly bound molecules such as van der Waals molecules are investigated by using sophisticated methods for electronic states, *i.e.*, multi-reference single and double excitation configuration interaction (MRSDCI) and multi-reference coupled pair approximation (MRCPA) calculations.

V-N-1 *Ab initio* Study of the van der Waals Molecule ArHF

GHOSH, Tapas Kumar; MIYOSHI, Eisaku; TANAKA, Kiyoshi¹
(¹Hokkaido Univ.)

Ab initio calculations were performed for the van der Waals complex ArHF using the multi-reference single and double excitation configuration interaction (MRSDCI) and multi-reference coupled pair approximation (MRCPA) methods to determine the spectroscopic parameters and potential energy surfaces of the ground X ¹Σ⁺ and first excited 2¹Σ⁺ states. The calculated ground-state equilibrium constants compared well with the available data. This is the first report of spectroscopic data for the excited state. Another subject of this study was the possibility of a fluorine anion from an excited ionic state (ArHF)^{*} produced by Ar colliding with an excited ionic state of HF. The excited 2¹Σ⁺ state is of ionic type (H⁺F⁻) and dissociates to a negative fluorine ion. This enlightens the photochemical reaction of the ionic excited HF with Ar correlating to the production of negative F ion:

**V-N-2 *Ab initio* Molecular Orbital Study of Fe(CO)_n (n = 1, 2 and 3)**

HONDA, Hiroaki¹; NORO, Takeshi¹; MIYOSHI, Eisaku
(¹Hokkaido Univ.)

Various unsaturated iron carbonyl complexes Fe(CO)_n (n = 1 to 4) have been produced by the UV photolysis of iron pentacarbonyl Fe(CO)₅.¹ Among them the spectroscopic studies of the FeCO radical has been extensively performed from both experimental and theoretical points of view and there have been a few experimental spectroscopic constants of Fe(CO)₂ and Fe(CO)₃.

Although there have been published several theoretical studies for Fe(CO)₂ and Fe(CO)₃, there are few comprehensive studies for the change of bonding nature in the Fe(CO)_n (n = 1 to 3) radicals. In this study we have carried out MCSCF calculations for the Fe(CO)_n (n = 1 to 3) to investigate the nature of bonding respect to change in the number of CO ligands. The calculated bond lengths of R(Fe-C) are reasonably in agreement with experimental values and more sophisticated theoretical results. From the Mulliken population analysis, the traditional donation and back donation mechanism is valid for FeCO through Fe(CO)₃.

Reference

1) K. Tanaka, K. Sakaguchi and T. Tanaka, *J. Chem. Phys.* **106**, 2118 (1997).

V-N-3 *Ab initio* Study on the Ground State of the C₃O₂ Molecule

MIYOSHI, Eisaku; SHIDA, Norihiro¹
(¹Nagoya Inst. Tech.)

[*Chem. Phys. Lett.* **303**, 50 (1999)]

Restricted Hartree-Fock (RHF) and single-reference coupled pair approximation (SRCPA) calculations were performed for the ground state of the C₃O₂ molecule. The SRCPA calculations revealed that C₃O₂ is quasi-linear with a global minimum in a W-shaped structure (C_{2v} symmetry) with ∠C-C-C = 153.6° and ∠C-C-O = 176.4°. To obtain the qualitatively correct description that the C₃O₂ molecule has a global minimum in the W-shaped structure, basis sets of higher quality than double-zeta with double polarization functions are indispensable. The observed very low frequency of 18.2 cm⁻¹ is not a fundamental vibrational frequency along the ν₇ mode, but should rather be assigned to the transition between two vibrational states which are split by the interaction of two ground vibrational state in the double minima.

V-N-4 On the Calculation of Binding Energy of the (C₆H₆)³⁺ Ion

GHOSH, Tapas Kumar; MIYOSHI, Eisaku

The benzene trimer cation, (C₆H₆)³⁺, has become an important system in the cluster ion spectroscopy because of the identification of core in the ion. It is yet controversial whether the benzene trimer cation has charge delocalized or localized structure. We performed *ab initio* CASSCF followed by MRSDCI as well as SRSDCI calculations for the benzene trimer cation (C₆H₆)³⁺ in its ground state assuming a sandwich-like structure. The total number of generated CSFs in MRSDCI calculations was 7,131,105. The equilibrium distances between two consecutive rings at the global minimum of the trimer cation in its ground state calculated by CASSCF in C_{2v} symmetry were 7.299 a.u. The dissociation energy (D_e) for the ground state of benzene trimer cation relative to (C₆H₆)²⁺ + C₆H₆ was calculated to be 195 meV at the CASSCF level and 349 meV at the MRSDCI including Davidson's correction in comparison to the experimental value (D₀) of 338 meV. The total binding energy relative to 2C₆H₆ + C₆H₆⁺ was calculated to be 757 meV at the MCSCF level and 984 meV at the MRSDCI including Davidson's correction, which is in agreement with a recent experimental upper limit of 990 ± 50 meV. It has been concluded from our calculation that in the trimer cation charge is localized at the central benzene ring, not that the charge is localized on a dimer core as was suggested by some experimentalists.

V-O Molecular Dynamics Study Using Potentials by *ab initio* Molecular Orbital Calculations

Using potentials obtained by *ab initio* molecular orbital calculations, molecular dynamics calculations were performed to investigate physical properties of liquid mercury.

V-O-1 Molecular Dynamics Study of Liquid Mercury in the Density Region between Metal and Nonmetal

SUMI, Tomonari; MIYOSHI, Eisaku; TANAKA, Kiyoshi¹

(¹Hokkaido Univ.)

[*Phys. Rev. B* **59**, 6153 (1999)]

We performed SDCI, SDCI(+Q), and CPA calculations for the ground $^1\Sigma_g^+$ state of Hg_2 incorporating the 5d and 6s electron correlations and major relativistic effects. The many-electron-excitation effect produces spectroscopic constants close to the experimental values. Although the metal-nonmetal (M-NM) transition can be explained as a simple band-crossing transition in one-electron theory, the many-electron-excitation effect is very important for describing the interaction between mercury atoms.

MD calculations for expanded liquid mercury were performed using the potential energy curve of Hg_2 , in the regions including the M-NM transition range. The volume (V) dependence of the thermal pressure coefficient, γ_v , and the internal pressure, P_0 , estimated by the MD calculations agree well with experimental results. Thus, many-body interactions or the qualitative change in the form of interatomic interactions arising from density dependence are not necessarily essential to explain the behavior of the γ_v vs. V and the P_0 vs. V curves. The change of calculated pair distribution function between metallic and nonmetallic state qualitatively demonstrates the change of experimental ones. The temperature dependence of the isochoric electrical conductivity was estimated using interatomic distances obtained from the calculated pair distribution functions. It was shown that the increase of the isochoric electrical conductivity accompanying an increase in temperature can be realized through the increase of the density of states at the Fermi energy. In the preceding paper,¹⁾ we reported that the MD calculations near the melting point using the potential curve of Hg_2 reproduce the cooperative motion corresponding to the collective short-wavelength excitations in the dynamic structure factor. These results suggest that pair-potential approximation using the potential curve of the dimeric molecule gives a good qualitative description of the metallic interatomic force for liquid mercury, and MD calculations using this approximation demonstrate the characteristic change of force fields between liquid metal and liquid semiconductor. However, the both γ_v vs. V and P_0 vs. V curves estimated by the MD calculations seem to deviate from the observed values slightly in the high-density metallic region. These differences between the observed and calculated values may be attributed to the lack of the many-body effects.

It has been pointed out²⁾ that the relative importance

of three-body interactions compared with two-body interactions in the liquid-vapor critical range for mercury is larger than for other van der Waals molecules. The boiling point determined by the present MD calculations is much higher than the observed value. This higher temperature should be corrected by considering three-body effects, such as the Axilrod-Teller interaction, because the three-body dispersion forces are repulsive while the two-body dispersion force is a long-range attractive force. It is interesting to determine the liquid-vapor coexistence curve with pair-potential approximation using the potential energy curve of Hg_2 and to investigate the contribution of three-body effects to the liquid-vapor transition phenomena, especially in liquid-vapor critical range.

References

- 1) T. Sumi, E. Miyoshi, Y. Sakai and O. Matsuoka, *Phys. Rev. B* **57**, 914 (1998).
- 2) M. W. Pestak, R. E. Goldstein, M. W. Chan, J. R. de Bruyn, D. A. Balzarini and N. W. Ashcroft, *Phys. Rev. B* **36**, 599 (1987).

V-O-2 The Liquid-Vapor Coexistence Curves of Fluid Mercury

SUMI, Tomonari; MIYOSHI, Eisaku

It has been known that the liquid-vapor coexistence curve of mercury is different from those of alkali metals (Rb, Cs) and inert gases (Ar, Xe).¹⁾ The followings have been established for these liquid-vapor coexistence curves and the rectilinear diameters, $r_d = (r_L + r_V)/2r_c$, where r_L , r_V , and r_c is the coexisting liquid density, vapor density, and the critical density, respectively: (1) The two phase region of mercury is narrower than those of alkali metals and inert gases; (2) The r_d of inert gases is a linear function of temperature, T , which is the law of rectilinear diameter, except for the near critical point, while the r_d of alkali metals and mercury deviate from the law of rectilinear diameter in wide temperature region. It has been suggested that the evidence in (2) might be attributed to many body effects.²⁾

We have performed molecular dynamics (MD) calculations for liquid mercury using the potential energy curve of dimeric mercury (Hg_2), which was obtained by molecular orbital calculations, in order to study the properties of mercury at the various temperature and density regions. In particular, the MD calculations using this approximation qualitatively reproduced the volume dependence of the thermal pressure coefficient and the internal pressure in the density regions including the metal-nonmetal transition range.³⁾ In this study, the MD calculations of fluid mercury are performed to determine the liquid-vapor phase transition points of mercury, and the relationship between the pair potential and liquid-vapor coexistence

curve is discussed.

The pair potential have been obtained from the CPA calculations developed by Tanaka and co-workers. The MD calculations were performed using a Verlet algorithm with 864 particles in an isothermal and isobaric ensemble with a time step of 0.005 fs. The physical quantities near the transition points were determined from the statistical averages over 2 000 000 to 10 000 000 intervals.

The results of MD calculations are as follows: (1) Our calculations qualitatively reproduced the liquid-vapor coexistence curve of mercury which is mentioned above; (2) Calculated r_d is not a linear function of T . Thus, our results suggest that the law of rectilinear diameter breaks down in the pair potential approximation.

References

- 1) F. Hensel, *J. Phys. C* **2**, SA33 (1990).
- 2) R. Goldstein and N. E. Ashcroft, *Phys. Rev. Lett.* **55**, 2164 (1985).
- 3) T. Sumi, E. Miyoshi and K. Tanaka, *Phys. Rev. B* **59**, 6153 (1999).

V-P Millimeter-Wave Spectroscopy Combined with Pulsed-Jet Expansion Technique for the Detection of the Novel Unstable Species and the van der Waals Mode Transitions of Molecular Clusters

Molecular clusters have inherently low-frequency vibrations, so called van der Waals (vdW) vibrational modes, which are characteristic of the weakly bound complexes. The frequency of the vdW mode usually falls in the far-infrared region (30–300 cm^{-1}). However, if a cluster is extremely floppy, it sometimes falls in the submillimeter-wave (SMMW) region below 30 cm^{-1} .

The ArHCN cluster is a typical example which has extremely low-frequency vdW bending vibrations. Although the frequency of the vdW stretching is estimated to be 23.8 cm^{-1} , those for the bending vibrations are calculated to be as low as 4–7 cm^{-1} . Following the observation of the pure rotational spectra in the microwave region below 20 GHz, the vdW bending transitions of ArHCN have been measured in the millimeter-wave region near 180 GHz by molecular beam electric resonance optothermal spectroscopy (EROS).

In this project, a millimeter-wave absorption spectrometer combined with pulsed-jet expansion technique has been devised and applied to the direct observation of the rovibrational transitions of the vdW bending band of molecular clusters. We have applied this technique to observe the vdW bending bands of the ArHCN ($j = 1-0$ and $2-1$) and ArDCN ($j = 1-0$) clusters as well as the ArHBr ($\Sigma_1-\Sigma_0$) and OCO-HF (1^1-0^0 (ν_b)) clusters.

In the supersonic jet expansions short lived species can survive thanks to the collision-less environment and ultra low rotational as well as vibrational temperature. The millimeter-wave spectrometer combined with supersonic jet nozzle and glow discharge electrodes, as well as the UV excimer laser photolysis devices, also have been set up for the detection of novel unstable species, such as radicals, molecular ions, and ionic and radical clusters.

V-P-1 Millimeter-Wave Spectroscopy of the van der Waals Bending Band of the ArDCN Cluster

BAILLEUX, Stephane; MIZOGUCHI, Asao; HARADA, Kensuke; BABA, Takeshi¹; SHIRASAKA, Mitsuaki¹; TANAKA, Keiichi²

(¹Kyushu Univ.; ²IMS and Kyushu Univ.)

Millimeter-wave absorption spectroscopy combined with pulsed-jet expansion technique was applied to the measurement of the rovibrational transitions in the van der Waals bending band of the ArDCN cluster in the frequency region of 182–294 GHz. Sixteen and thirty-seven rovibrational lines were observed for the $\Sigma_1-\Sigma_0$ and $\Pi_1-\Sigma_0$ bands, respectively, split into hyperfine structure due to the nitrogen nucleus. The spectrum of the $R(1)$ line of the $\Sigma_1-\Sigma_0$ band observed at 196 GHz is shown in Figure 1.

An accurate set of molecular constants, including the band origins, rotational constants, quadrupole coupling constants, and the Coriolis coupling constant between the Σ_1 and Π_1 bending substates, was determined. The rotational and quadrupole coupling constants for the excited states are much different from those of the ground state indicating the change in average molecular structure, from the linear form in the ground state to the T-shaped form in the first excited ($j = 1$) state. The band origins for the $\Sigma_1-\Sigma_0$ and $\Pi_1-\Sigma_0$ bands, 189.017 391 (7) GHz and 195.550 737 (12) GHz, are larger by 24.126 596 (9) and 13.566 315(16) GHz than the corresponding values of ArHCN.¹ The abnormal isotopic effect on the vibrational frequencies is attributed to the characteristic potential energy surface of ArH(D)CN, which have two minima corresponding to linear and T-shaped configurations with similar well depth and connected with a shallow channel. The determined molecular constants were compared with those calculated with potential energy surface given by CCSD(T) level *ab initio* calculation.²

References

- 1) K. Uemura, A. Hara and K. Tanaka, *J. Chem. Phys.* **104**, 9747 (1996).
- 2) S. M. Cybulski, J. Couvillion, J. Klos and G. Chalasinski, *J. Chem. Phys.* **110**, 1416 (1999).

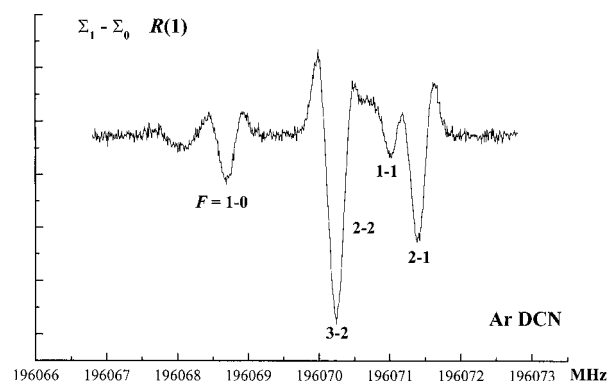


Figure 1. Hyperfine structure of the $R(1)$ line of the $\Sigma_1-\Sigma_0$ subband of the $j = 1-0$ vdW bending band of ArDCN.

V-P-2 Direct Observation of the van der Waals Bending Hot Bands of the Ar-HCN Cluster by Millimeter-Wave Spectroscopy

MIZOGUCHI, Asao; HARADA, Kensuke; TANAKA, Keiichi¹

(¹IMS and Kyushu Univ.)

The previous spectroscopic studies of the “ball and ball”-type cluster such as the Ar-HCl and Ar-H₂O clusters gave the computational techniques for evaluating the experimental potential energy surface (PES). As a next target, many experimentalists and theoreticians have investigated the Ar-HCN cluster because it is one of the simplest “ball and rod”-type cluster.

Since the first observation of the rotational spectrum of Ar-HCN was carried out by Leopold *et al.*,¹ many

studies have been reported. The observation of the vdW vibration is important to determine the intermolecular PES. The vdW bending fundamental bands were observed by Drucker *et al.*²⁾ These experimental results showed that this cluster has abnormally large centrifugal distortion constants and isotopic effect on the molecular constants of the normal and deuterated species. *Ab initio* calculation by Tao *et al.*³⁾ and Cybulski *et al.*⁴⁾ showed that this abnormality is due to the characteristic PES of Ar-HCN (Figure 1), which has large angular-radial coupling and anisotropy in the vdW vibration.

In the present work, the vdW bending hot bands of Ar-HCN have been observed by using the millimeter-wave absorption spectroscopy combined with the pulsed supersonic jet expansion technique. In the frequency region of 150–290 GHz, the six bands correlated to the $j = 2-1$ transition in the free rotor limit were assigned and least-squares fitted simultaneously to the effective Hamiltonian including the Coriolis interaction (Figure 2). The order of the sublevels in the $j = 2$ state is reversed to that of $j = 1$ state, which is consistent with the vibrational analysis with the PES by Cybulski *et al.* Since the observed rotational constants in the $j = 2$ state have almost the same values as those of the $j = 1$ state, the average distance between Ar and center of mass of HCN in the $j = 2$ state is not changed so much. The signs of nuclear quadrupole coupling constants in the $j = 2$ state are the same as those of the coupling constants predicted in the free rotor limit.

References

- 1) K. R. Leopold, G. T. Fraser, F. J. Lin, D. D. Nelson, Jr. and W. Klemperer, *J. Chem. Phys.* **81**, 4922 (1984).
- 2) S. Drucker, A. L. Cooksy and W. Klemperer, *J. Chem. Phys.* **98**, 5158 (1993).
- 3) F. M. Tao, S. Drucker and W. Klemperer, *J. Chem. Phys.* **102**, 7289 (1995).
- 4) S. M. Cybulski, J. Couvillion, J. Kłots and G. Chałasiński, *J. Chem. Phys.* **110**, 1416 (1999).

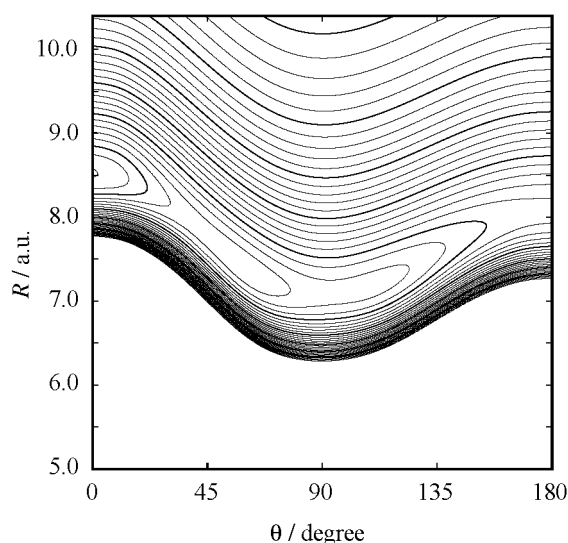


Figure 1. The PES of Ar-HCN. This PES was obtained by the high-level *ab initio* calculation with CCSD(T)/aug-cc-pVTZ+bf method.⁴⁾

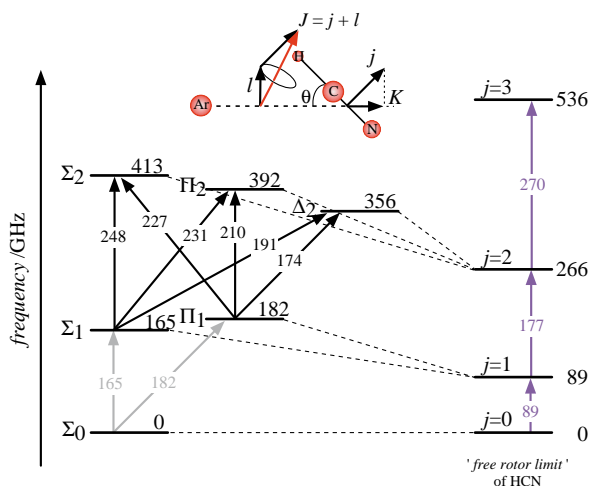


Figure 2. Energy level diagram of Ar-HCN. Since each vibrational energy level correlates to the free rotor energy levels of HCN, the vdW vibrational levels are labeled with $|K|_j$.

V-P-3 Submillimeter-Wave Spectroscopy of the van der Waals Bending Band of Ar-HBr

HARADA, Kensuke; MIZOGUCHI, Asao; TANAKA, Keiichi¹

(¹IMS and Kyushu Univ.)

The Ar-HBr cluster has a large amplitude intermolecular bending motion. It has nearly a “linear” structure of Ar-HBr in the ground state (Σ_0 state), while nearly an “anti-linear” structure of Ar-BrH in the first excited state (Σ_1 state) by the calculation of Hutson.¹⁾ Recently, the excited states of the van der Waals vibrations were observed by infrared²⁾ and far infrared³⁾ laser spectroscopy. The energy difference between the Σ_1 and Σ_0 state was determined to be 10.995 cm^{-1} from the combination difference of the infrared data.²⁾ In the present study, we have observed direct submillimeter-wave transitions of the $\Sigma_1-\Sigma_0$ band of Ar-HBr generated in a pulsed supersonic jet expansion.

The millimeter-wave jet spectrometer have been used for the experiment. The 8 atm mixed gas of 1% HBr, 49% Ar, and 50% Ne was injected to the vacuum chamber from a pulsed nozzle. In the frequency region of 318–335 GHz, the 14 rovibrational transition of P(12)-P(1), R(0), and R(1) have been observed for both Ar-H⁷⁹Br and Ar-H⁸¹Br isotopic species. Since the van der Waals bond length in the Σ_1 states is 0.2 \AA shorter than that in the ground state, the spectrum has a band head at P branch side. Figure 1 shows the P(8) and P(10) lines near the band head at 319 GHz, split due to the nuclear quadrupole interaction of the bromine nucleus.

The eQq constants in the the Σ_1 state were determined to be 260.90(12) and 217.854(98) MHz for Ar-H⁷⁹Br and Ar-H⁸¹Br, respectively, which are 51% larger than the values in the ground state. The rotational dependence of the eQq constant, eQq_J in the the Σ_1 state has reverse sign to that in the ground state. The big change of the eQq constant and the reverse sign of the eQq_J indicate that the cluster is in the different minima of the potential surface at the “linear” and “anti-linear” structures, in the Σ_0 and Σ_1 state, respectively.

References

- 1) J. M. Hutson, *J. Chem. Phys.* **91**, 4455 (1989).
- 2) J. Han, A. L. McIntosh, Z. Wang, R. R. Lucchese and J. W. Bevan, *Chem. Phys. Lett.* **265**, 209 (1997).
- 3) D. W. Firth, M. A. Dvorak, S. W. Reeve, R. S. Ford and K. R. Leopold, *Chem. Phys. Lett.* **168**, 161 (1990).

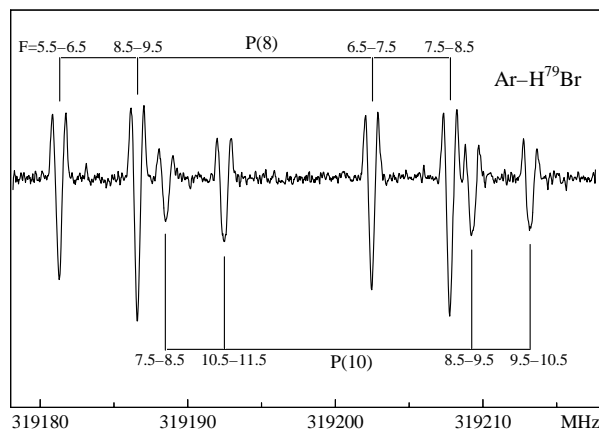


Figure 1. The observed spectrum of the $\Sigma_1-\Sigma_0$ vdW bending band of Ar-HBr.

V-P-4 Millimeter-Wave Spectroscopy of the van der Waals Bending Band of OCO-HF with a Supersonic Jet Expansion Technique

HARADA, Kensuke; ISHIGURO, Masazumi¹; TANAKA, Takehiko¹; TANAKA, Keichi²
(¹Kyushu Univ.; ²IMS and Kyushu Univ.)

The OCO-HF is a hydrogen-bonded quasi-linear cluster with a dissociation energy of 672 cm^{-1} . The intermolecular potential is double minimum at a bend structure of the COH angle of 22° and a potential barrier of about 1 cm^{-1} is expected in the linear configuration.¹⁾ The rotational spectrum²⁾ and infrared spectrum³⁾ have been already reported. In the present study, we have measured the van der Waals (vdW) bending 1^1-0^0 (ν_b^1) band by the millimeter wave jet spectroscopy.

The 8 atm mixed gas of 1% HF, 5% CO₂, 31% Ar, and 63% Ne was injected into the vacuum chamber by a pulsed nozzle. In the 250–325 GHz region, 30 rovibrational transitions, P(2)-P(5), Q(1)-Q(15), and R(0)-R(10), were assigned to the 1^1-0^0 (ν_b^1) fundamental band. Figure 1 shows the stick diagram of the observed spectrum. The band has intense Q and R branch lines, while the P branch lines are rather weak.

An usual linear molecule Hamiltonian with the (2,2) interaction was used for the analysis. The band origin of the 1^1-0^0 band was determined to be 272548.8017 (49) MHz. The rotational constant, centrifugal distortion constant, *l*-type doubling constant, and its higher order term were determined precisely. In order to determine the two dimensional intermolecular bending potential surface, the measurement of the vdW hot band and vdW band of the deuterated species will be important.

References

- 1) D. J. Nesbitt and C. M. Lovejoy, *J. Chem. Phys.* **96**, 5712 (1992).
- 2) F. A. Baiocchi, T. A. Dixon, C. H. Joyner and W.

Klemperer, *J. Chem. Phys.* **74**, 6544 (1981).

- 3) D. J. Nesbitt and C. M. Lovejoy, *J. Chem. Phys.* **93**, 7716 (1990).

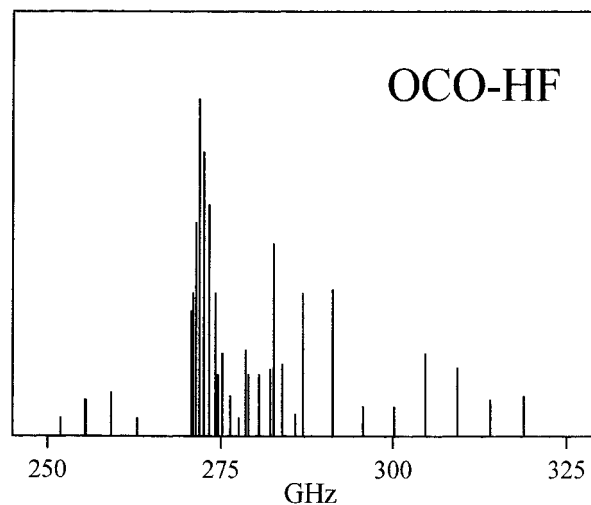


Figure 1. The stick diagram of the observed spectrum of the vdW bending band of OCO-HF.

V-Q Ion-Molecule Reactions in the Troposphere

Ion chemistry in the troposphere is the most complicated among all level of earth's atmosphere because of the presence of a variety of trace compounds. We have been studying ion-molecule reactions in the troposphere by investigating ion mobility distribution and its dependence on reaction time, pressure and temperature using an ion mobility spectrometer.^{1,2)} In order to confirm the ion-molecule reactions occurring in the troposphere, we developed a high-resolution ion mobility/mass spectrometer which is capable of chemical identification of ion species forming ion peaks in mobility spectra. Using this spectrometer, we investigate the ion processes in conditioned laboratory air as well as in natural air.

References

- 1) K. Nagato and T. Ogawa, *J. Geophys. Res.* **103**, 13917 (1998).
- 2) K. Nagato, D. J. Tanner, H. R. Friedli and F. L. Eisele, *J. Geophys. Res.* **104**, 3471 (1999).

V-Q-1 Measurements of Mobility and Mass Spectra of Tropospheric Ions

NAGATO, Kenkichi

We have developed a high-resolution ion mobility/mass spectrometer that can make simultaneous measurements of mobility and mass spectra of cluster ions generated by ion-molecule reactions under atmospheric pressure. The spectrometer consists of a drift tube, a mass analyzer, and an interface chamber between the drift tube and the mass analyzer. Both positive and negative ions, which are generated by irradiation of laboratory air with an americium source, are investigated by measuring mobility spectra, mass spectra, and mass-resolved mobility spectra. The results provide new information on the tropospheric ion evolution. In the positive ion spectra, ammonium ions dominate at around a few tenths of milliseconds after ionization. Then, they are converted into other ion species that have higher proton affinities than that of ammonia. Such ion species include pyridine, methylpyridine, methylamine, dimethylamine, trimethylamine, and isobutylamine. In addition, several ions are found in the mass spectra at masses 135, 149, 152, and 279, which have not been identified. In the negative ion mass spectra, we found new ion species at masses 45, 46, and 89, which were identified as ions of formic acid, nitrous acid, and oxalic acid, respectively.